Published June 30, 2014

Pom1 regulates the assembly of Cdr2–Mid1 cortical nodes for robust spatial control of cytokinesis

Sergio A. Rincon,[1,3] Payal Bhatia,[4] Claudia Bicho,[5] Mercè Guzman-Vendrell,[1,3] Vincent Fraisier,[1,3] Weronika E. Borek,[5] Flavia de Lima Alves,[5] Florent Dingli,[1,2] Damarys Loew,[1,2] Juri Rappsilber,[5] Kenneth E. Sawin,[5] Sophie G. Martin,[4] and Anne Paoletti[1,3]

[1]Centre de Recherche and [2]Laboratory of Mass Spectrometry and Proteomics, Institut Curie, F-75248 Paris, France
[3]Centre National de la Recherche Scientifique, Unite Mixte de Recherche 144, F-75248 Paris, France
[4]Department of Fundamental Microbiology, University of Lausanne, Lausanne CH-1015, Switzerland
[5]Wellcome Trust Centre for Cell Biology, University of Edinburgh, Edinburgh EH9 3JR, Scotland, UK

Proper division plane positioning is essential to achieve faithful DNA segregation and to control daughter cell size, positioning, or fate within tissues. In *Schizosaccharomyces pombe*, division plane positioning is controlled positively by export of the division plane positioning factor Mid1/anillin from the nucleus and negatively by the Pom1/DYRK (dual-specificity tyrosine-regulated kinase) gradients emanating from cell tips. Pom1 restricts to the cell middle cortical cytokinetic ring precursor nodes organized by the SAD-like kinase Cdr2 and Mid1/anillin through an unknown mechanism. In this study, we show that Pom1 modulates Cdr2 association with membranes by phosphorylation of a basic region cooperating with the lipid-binding KA-1 domain. Pom1 also inhibits Cdr2 interaction with Mid1, reducing its clustering ability, possibly by down-regulation of Cdr2 kinase activity. We propose that the dual regulation exerted by Pom1 on Cdr2 prevents Cdr2 assembly into stable nodes in the cell tip region where Pom1 concentration is high, which ensures proper positioning of cytokinetic ring precursors at the cell geometrical center and robust and accurate division plane positioning.

Introduction

Close coordination between chromosome segregation and cytokinesis is crucial for proper cell division and inheritance of the genetic material. For example, division plane positioning defects can lead to chromosome segregation anomalies and aneuploidy and can also perturb cell organization or cell lineage during early development of multicellular organisms.

In animal cells, division plane positioning is regulated by positive and negative spatial cues emanating from the spindle midzone and spindle poles, respectively, ensuring a direct spatial coordination between chromosome segregation and cytokinesis (Balasubramanian et al., 2012; Fededa and Gerlich, 2012; Green et al., 2012; White and Glotzer, 2012). Similarly, in the fission yeast *Schizosaccharomyces pombe*, a combination of positive and negative spatial cues act to establish the position of the division plane in the middle of this rod-shaped single-celled organism (Oliferenko et al., 2009; Almonacid and Paoletti, 2010; Rincon and Paoletti, 2012).

Positive signaling of the division plane involves the nuclear export of the anillin-like protein Mid1 (Sohrmann et al., 1996), which spatially couples the position of the nucleus during interphase to the assembly site of the cytokinetic ring (Daga and Chang, 2005; Almonacid et al., 2009). This mechanism leads to Mid1 accumulation on juxtanuclear regions of the cortex, where Mid1 forms cytokinetic ring precursor nodes and, upon activation by the polo-like kinase Plo1, promotes the sequential recruitment of essential components of the contractile ring (Bathe and Chang, 2010; Laporte et al., 2010; Pollard and Wu, 2010; Almonacid et al., 2011; Goyal et al., 2011; Lee et al., 2012).

This mitotic recruitment phase starts with the recruitment of myosin II in an IQGAP (IQ domain GTPase-activating protein)/Rng2-dependent manner followed by the F-BAR (FER/CIP4 homology domain-Bin-Amphiphysin-Rvs–like protein) protein

Correspondence to Anne Paoletti: anne.paoletti@curie.fr

C. Bicho's present address is Dept. of Cell and Tissue Biology, University of California, San Francisco Medical Center, San Francisco, CA 94143.

Abbreviations used in this paper: DYRK, dual-specificity tyrosine-regulated kinase; MBP, maltose-binding protein; MS, mass spectrometry; TEV, tobacco etch virus.

Supplemental Material can be found at:
http://jcb.rupress.org/content/suppl/2014/06/26/jcb.201311097.DC1.html

The Rockefeller University Press $30.00
J. Cell Biol. Vol. 206 No. 1 61–77
www.jcb.org/cgi/doi/10.1083/jcb.201311097

Published June 30, 2014

Cdc15 and F-actin nucleator Cdc12 (Almonacid et al., 2011; Laporte et al., 2011; Padmanabhan et al., 2011). Compaction of mature ring precursors driven by actomyosin forces then leads to the formation of a medially placed contractile ring (Vavylonis et al., 2008; Ojkic et al., 2011).

In *mid1Δ* cells, actomyosin strands or contractile rings assemble at random positions within the cell. Contractile ring assembly then depends on the septation initiation network (Hachet and Simanis, 2008; Huang et al., 2008), which regulates Cdc15 conformation through Clp1-dependent dephosphorylation and inhibits Cdc12 multimerization by Sid2-dependent phosphorylation (Roberts-Galbraith et al., 2010; Bohnert et al., 2013). Nevertheless, *mid1* mutation or deletion yields extensive cell death in the cell population (Chang et al., 1996; Sohrmann et al., 1996), indicating that Mid1-dependent regulation of the contractile ring position contributes to cell survival and proper segregation of chromosomes between sister cells.

A parallel pathway regulating division plane positioning in fission yeast relies on a negative cue that emanates from cell tips in the form of spatial gradients of the dual-specificity tyrosine-regulated kinase (DYRK) family kinase Pom1 (Bähler and Pringle, 1998; Celton-Morizur et al., 2006; Padte et al., 2006). Pom1 membrane diffusion-based gradients are nucleated by microtubule-dependent delivery of the Tea protein complexes to the cell tips where they anchor a PP1 phosphatase (Alvarez-Tabarés et al., 2007; Martin, 2009; Hachet et al., 2012). PP1 reverses Pom1 autophosphorylation on its membrane-anchoring domain, which otherwise promotes a progressive detachment of Pom1 from the plasma membrane as Pom1 diffuses away from the cell tip region (Hachet et al., 2011; Saunders et al., 2012). Pom1, in turn, has been shown to control the distribution of Cdr2 (Breeding et al., 1998; Kanoh and Russell, 1998), a conserved member of the Brsk/SAD (synapses of the amphid defective)/Septin kinase subfamily of AMP kinase–like kinases that assembles into nodes on the cortex (Morrell et al., 2004). In *pom1Δ* cells, growth is monopolar, and Cdr2 nodes, normally restricted to the medial cortex, invade the nongrowing cell tip (Martin and Berthelot-Grosjean, 2009; Moseley et al., 2009). Surprisingly, Cdr2 nodes remain excluded from the growing tip, but the mechanism of this additional Pom1-independent regulation remains unknown.

Importantly, Cdr2 nodes recruit Mid1 to the medial cortex during interphase and gradually collect a series of nonessential ring components (e.g., Blt1, Gef2, and Nod1) released from the previous division site (Almonacid et al., 2009; Moseley et al., 2009; Ye et al., 2012; Guzman-Vendrell et al., 2013; Jourdain et al., 2013; Zhu et al., 2013; Akamatsu et al., 2014). As a result, in *pom1Δ* cells, the distribution of contractile ring precursors is perturbed, leading to asymmetric division (Celton-Morizur et al., 2006; Padte et al., 2006). Thus, Pom1-dependent regulation of Cdr2 node distribution on the cortex allows prepositioning of Mid1 to the geometric center of the cell. This pathway, which is necessary to promote the formation of equally sized sister cells when Mid1 shuttling in the nucleus is impaired, contributes to the robustness and accuracy of division plane positioning in wild-type cells.

Interestingly, Pom1 and Cdr2 regulate not only division plane positioning but also division timing by modulation of Cdk1 activity (Martin and Berthelot-Grosjean, 2009; Moseley et al., 2009). Cdr2 cortical nodes indeed contain several regulators of mitotic entry, including Cdr2 itself, which acts as a Wee1-inhibitory kinase (Breeding et al., 1998; Kanoh and Russell, 1998), the Cdr1/Nim1 kinase homologous to Cdr2 (Russell and Nurse, 1987a; Coleman et al., 1993; Parker et al., 1993; Wu and Russell, 1993), and the Cdk1 inhibitor Wee1 (Russell and Nurse, 1987b; Moseley et al., 2009). Collectively, these constitute a Wee1-inhibitory network. In the proposed models, Pom1 maintains this Wee1-inhibitory network inactive in short cells, preventing mitotic entry until a critical length has been reached (Martin and Berthelot-Grosjean, 2009; Moseley et al., 2009). Whether the Pom1–Cdr2 pathway constitutes an active cell size sensor has nevertheless been recently challenged (Wood and Nurse, 2013). Recent data indicate that this role of Pom1 in regulating division timing is genetically separable from its role in division plane positioning (Bhatia et al., 2014) and involves Pom1 indirectly regulating the kinase activity of Cdr2 by phosphorylation of the C-terminal tail, which antagonizes the phosphorylation of Cdr2 T loop by the calcium/calmodulin-dependent protein kinase kinase Ssp1 (Bhatia et al., 2014; Deng et al., 2014).

In contrast, the molecular mechanisms underlying how Pom1 gradients negatively regulate Cdr2 node distribution are not understood. Here, we have deciphered the mechanisms by which Cdr2 assembles into nodes on the cell cortex and dissected how the spatial information of Pom1 gradients is transduced into functional outputs for division plane positioning. Similar to Pom1 gradients, several dynamic gradients are known to provide spatial subcellular information to establish stable domains with specific biochemical activities (Fuller, 2010). Yet, in most cases, how the spatial information is transduced to target activities remains unclear. Our study provides a first mechanistic model that might be relevant to other spatial regulatory events involving membrane gradients.

Results

The Cdr2 KA-1 domain and a neighboring basic region cooperate to promote Cdr2 membrane binding

To understand how Pom1 constrains Cdr2 node distribution at the cell medial cortex to predefine the division plane, we first studied how Cdr2 associates with the cortex. A large region of Cdr2 of ∼500 amino acids C terminal to the kinase domain was previously shown to be necessary and sufficient for Cdr2 cortical localization (Morrell et al., 2004). This region includes a predicted structured domain of ∼130 amino acids composed of three putative α helices and five β sheets (Fig. 1 A) with low similarity to the recently described lipid-binding KA-1 domain of Kcc4, a kinase homologous to Cdr2 in *Saccharomyces cerevisiae* (Moravcevic et al., 2010). Mutations in any of the three α helices completely detached Cdr2 from the cortex (Fig. S1 A) and induced Cdr2 relocalization to the nucleus, indicating that the lipid-binding function of this domain may be conserved.

Surprisingly, homology modeling of the Cdr2 KA-1 domain, based on the crystal structure of Kcc4 KA-1 (Fig. 1 B),

Published June 30, 2014

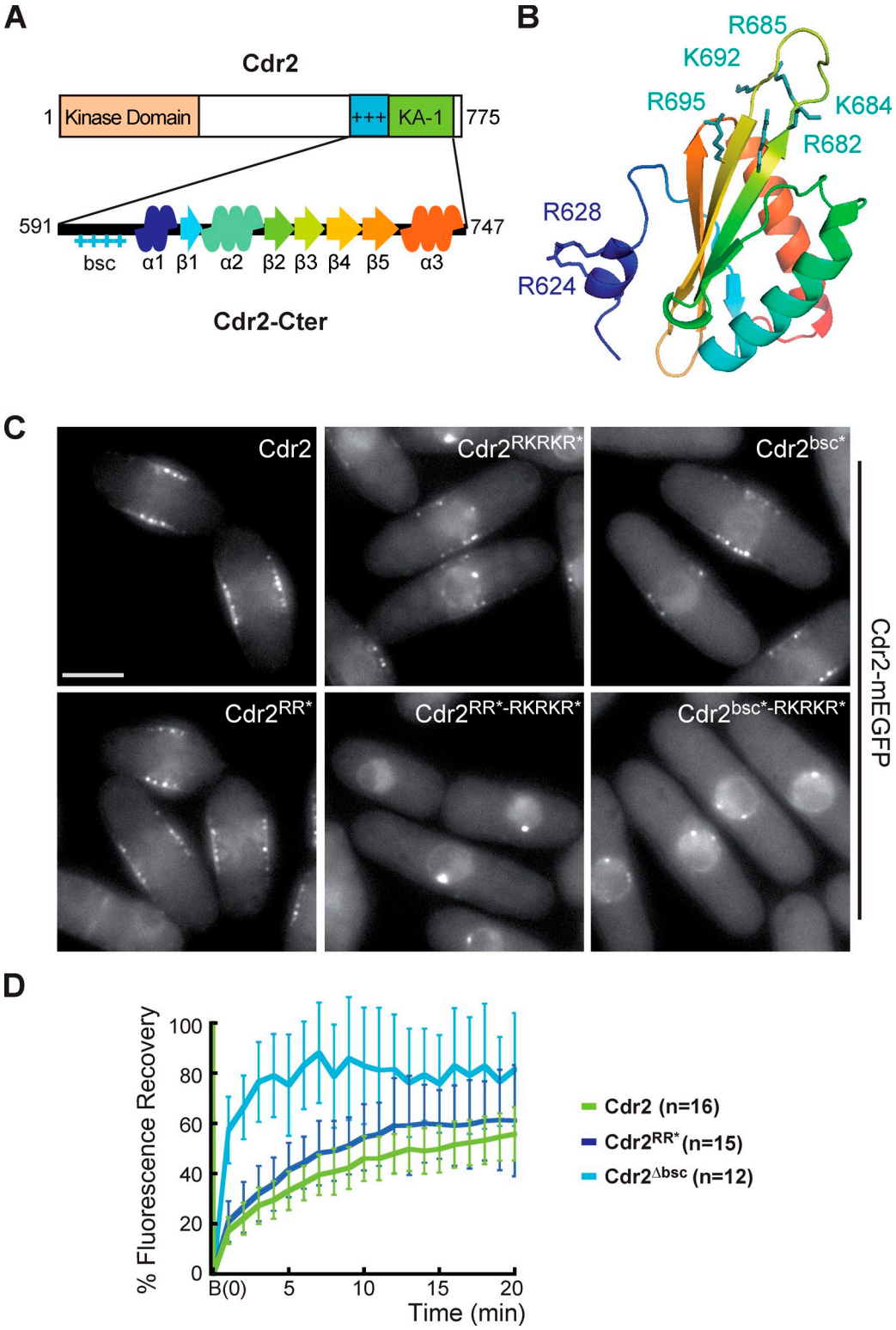

Figure 1. **C-terminal KA-1 domain and basic motif mediate Cdr2 membrane binding.** (A) Schematic representation of full-length Cdr2 (top) and Cdr2 C-terminal cortex-anchoring domain (Cdr2-Cter, residues 591–747; bottom) composed of a basic region (blue) and a KA-1 domain (green on top and rainbow on the bottom). Predicted α helices and β sheets of the KA-1 domain are shown. (B) Structural model of Cdr2 KA-1 domain derived from the *S. cerevisiae* Kcc4 KA-1 crystal structure (Protein Data Bank accession no. 3OST). Seven positively charged residues sticking out of the domain are highlighted in blue. (C) Epifluorescence medial plane images of mEGFP-tagged Cdr2 mutants of the positively charged residues of Cdr2 KA-1 shown in B ($Cdr2^{RR*}$: R624Q and R628Q; $Cdr2^{RKRKR*}$: R682Q, K684N, R685Q, K692N, and R695Q; $Cdr2^{RR*\text{-}RKRKR*}$: combination of all mutations), in the basic region upstream of Cdr2 KA-1 ($Cdr2^{bsc*}$: K598N, H599Q, R600Q, R601Q, R602Q, K612N, K613N, and K614N), or in both ($Cdr2^{bsc*\text{-}RKRKR*}$). Bar, 5 µm. (D) Mean FRAP of mEGFP-tagged Cdr2 or $Cdr2^{RR*}$ and $Cdr2^{\Delta bsc}$ mutants on the medial cortex as indicated. Error bars show SDs. Cdr2 $t_{1/2}$ = ∼3 min; $Cdr2^{RR*}$ $t_{1/2}$ = ∼3 min; $Cdr2^{bsc\Delta}$ $t_{1/2}$ < 1 min. B, bleach.

Published June 30, 2014

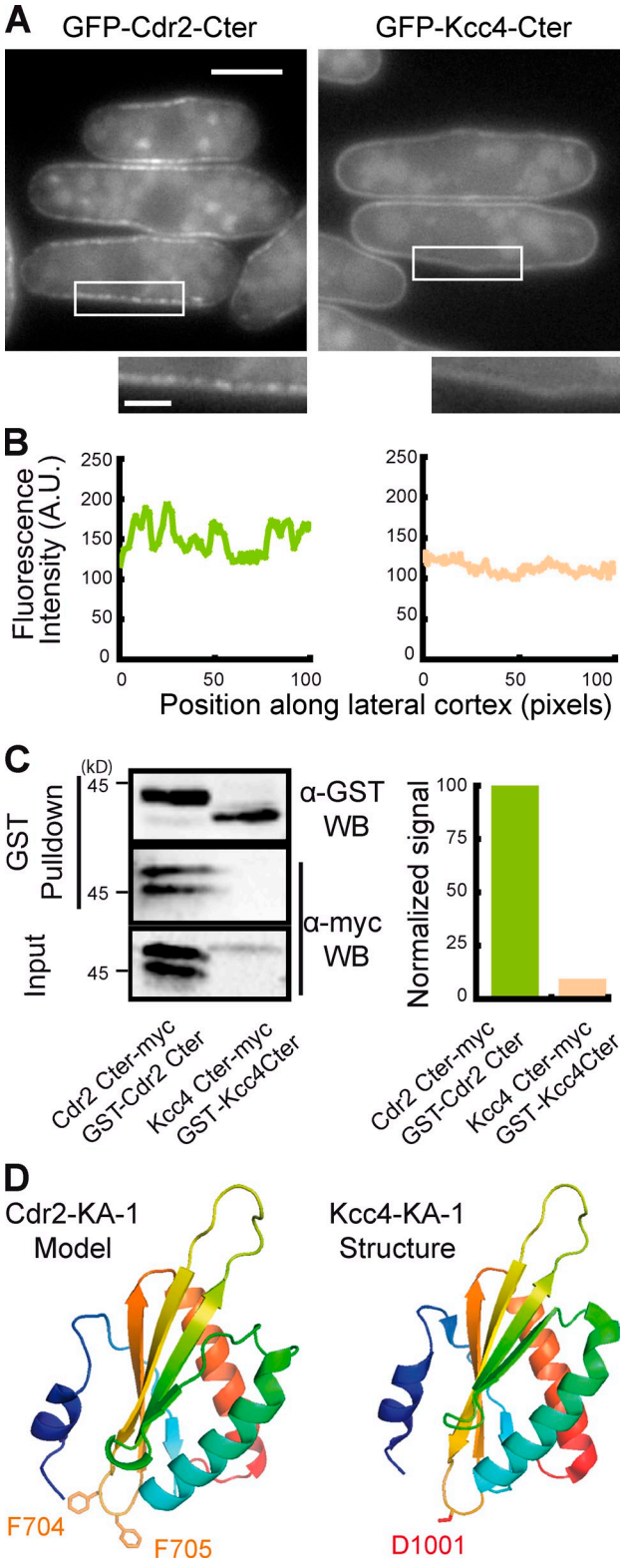

Figure 2. **Clustering properties of the Cdr2-Cter domain.** (A, top) Medial plane epifluorescence images of GFP–Cdr2-Cter (residues 591–747) and GFP–Kcc4-Cter (residues 893–1,037). Bar, 5 µm. (bottom) 1.75× magnification of boxed regions. Bar, 1 µm. (B) Fluorescence intensity along the cortex in regions boxed in A, representative of the cell population. (C) Pull-down assay between differentially tagged Cdr2-Cter or Kcc4-Cter. Overexpressed GST–Cdr2-Cter or GST–Kcc4-Cter was coupled to glutathione beads and mixed with extracts of cells expressing Cdr2-Cter–myc$_{12}$ or Kcc4-Cter–myc$_{12}$, respectively. Cdr2-Cter and Kcc4-Cter were revealed in input and pull-down fractions with anti-GST or antimyc antibodies. (right) Normalized Cter-myc signals in GST pull-down measured in two independent experiments. Molecular masses are indicated. (D) Cdr2 KA-1 model highlighting the two hydrophobic residues of the β4–β5 loop (F704 and F705) and the Kcc4 KA-1 structure 3OST (Moravcevic et al., 2010), in which the equivalent loop contains a charged residue (D1001) surrounded by two neutral residues (G1000 and G1002; not depicted). A.U., arbitrary unit; WB, Western blot.

revealed that surface-exposed basic residues mediating the electrostatic interactions with acidic phospholipids in Kcc4 KA-1 (Moravcevic et al., 2010) were not conserved in Cdr2 KA-1 (Fig. S1 B). In addition, some hydrophobic residues of the β3–β4 hydrophobic loop proposed to insert into the lipid bilayer were replaced by nonhydrophobic residues. Instead, we identified a cluster of surface-exposed basic residues in β3, β4, and the β3–β4 loop (R682, K684, R685, K692, and R695). Mutagenesis of these basic residues to noncharged polar amino acids (N or Q) showed that these residues have an important role in targeting Cdr2 to the cortex (Fig. 1 C). Mutations of two other basic residues from helix α1 (R624 and R628) did not affect Cdr2 association with the cortex on their own but led to a complete detachment when combined with mutations of the aforementioned five basic residues. Thus, a series of surface-exposed basic residues in Cdr2 KA-1 may cooperatively establish electrostatic interactions with negatively charged phospholipids.

The Cdr2 KA-1 domain is preceded by a basic motif (8 out of 17 positively charged residues; Fig. 1 A), whose deletion, or mutation of basic residues, resulted in a partial delocalization of Cdr2 from the cortex and appearance of a nuclear pool (Figs. 1 C and S1 A). In combination with mutation of the five basic residues close to the β3–β4 loop, this led to complete detachment of Cdr2 from the cortex. Thus, the basic motif cooperates with Cdr2 KA-1 to promote Cdr2 anchoring at the cortex. FRAP experiments further revealed that the localization defects observed in the various cortex-anchoring mutants described in this paper correlated with increased dynamic exchange of Cdr2 on the cortex (Fig. 1 D). These mutants also produced longer cells, with stronger Cdr2 localization defects correlating with longer delays in mitotic entry (Table S3), indicating that Cdr2 cortical localization is crucial for its function.

Cdr2 clustering involves both the KA-1 domain and Cdr2 N-terminal interaction with Mid1

A C-terminal region composed of the Cdr2 basic motif and KA-1 domain (residues 591–747), hereafter called Cdr2-Cter, was sufficient for cortex binding (Fig. 2 A). Similar to the Kcc4 KA-1 domain (Moravcevic et al., 2010), recombinant Cdr2-Cter also bound in vitro on lipid strips to phosphatidylserine, a major acidic phospholipid of the plasma membrane (Fig. S1 C). We also observed minor binding to phosphatidic acid and cardiolipin but not to phosphoinositides. Thus, Cdr2-Cter is necessary and sufficient for localization to the plasma membrane.

Interestingly, Cdr2-Cter formed small clusters on the medial cortex in contrast to the equivalent C-terminal domain of

Published June 30, 2014

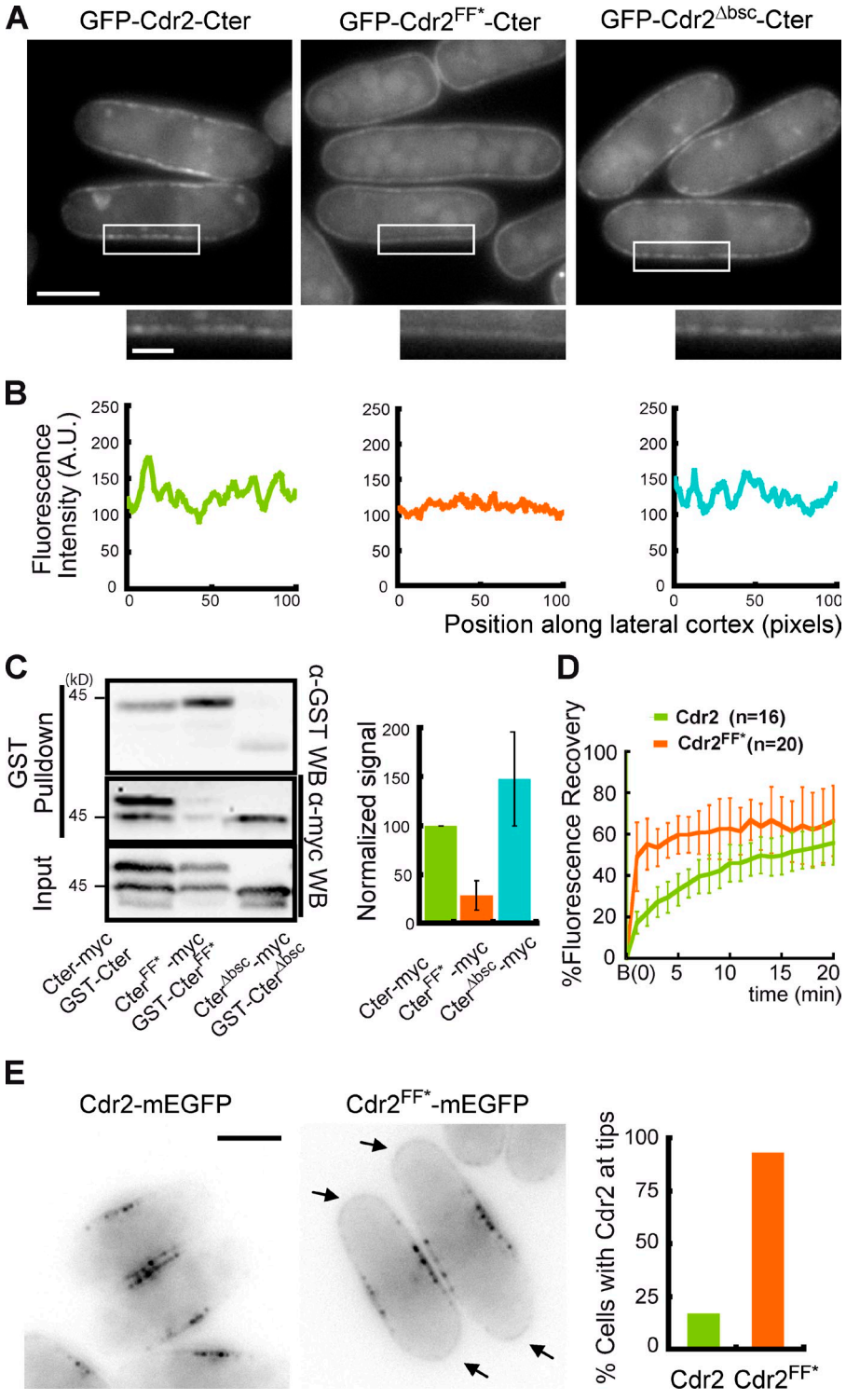

Figure 3. **Cdr2 hydrophobic β4–β5 loop regulates clustering.** (A) Localization of GFP-tagged Cdr2-Cter, Cdr2-Cter mutated in the F residues of the β4–β5 loop (Cdr2-Cter^{FF*}: F704D and F705D), or Cdr2-Cter$^{\Delta bsc}$. Bar, 5 µm. (bottom) 1.75× magnification of the boxed regions. Bar, 1 µm. (B) Fluorescence intensity along the cortex in regions boxed in A, representative of the cell population. (C) Pull-down assay between differentially tagged Cdr2-Cter, Cdr2-Cter^{FF*}, or Cdr2-Cter$^{\Delta bsc}$. Overexpressed GST–Cdr2-Cter, GST–Cdr2-Cter^{FF*}, or GST–Cdr2-Cter$^{\Delta bsc}$ were coupled to glutathione beads and mixed with extracts of cells expressing Cdr2-Cter–myc$_{12}$, Cdr2-Cter^{FF*}–myc$_{12}$, or Cdr2-Cter$^{\Delta bsc*}$–myc$_{12}$, respectively. Cdr2-Cter was revealed in input and pull-down fractions with anti-GST or anti-myc antibodies. (right) Normalized Cter-myc signals in GST pull-down measured in three independent experiments. Molecular masses are indicated. Error bars show SDs. (D) Mean FRAP of mEGFP-tagged Cdr2 and Cdr2^{FF*} mutant on the medial cortex as indicated. Error bars show SDs. Cdr2 $t_{1/2}$ = ∼3 min; Cdr2^{FF*} $t_{1/2}$ < 1 min. (E) Localization of mEGFP-tagged Cdr2 or Cdr2^{FF*}. Arrows show cell tip localization of Cdr2^{FF*}. Inverted black and white pictures are depicted. Bar, 5 µm. (right) Percentage of cells with Cdr2 or Cdr2^{FF*} detected at cell tips. n > 80 cells. A.U., arbitrary unit; B, bleach; WB, Western blot.

Kcc4, which was distributed homogeneously on the cortex when expressed in fission yeast (Fig. 2, A and B). This suggested to us that Cdr2 KA-1 may have unique oligomerization properties, not shared with Kcc4 KA-1, which may contribute to Cdr2 assembly into nodes and also allow multivalent membrane binding with high avidity (Lemmon, 2008). Accordingly, we found that differentially tagged wild-type Cdr2-Cter molecules interacted in pull-down experiments, whereas corresponding Kcc4-Cter failed to do so (Fig. 2 C).

Comparing our Cdr2 KA-1 structural model to the Kcc4 crystallographic structure, we found that the β4–β5 loop of the Cdr2 KA-1, opposite to the membrane-binding surface, is very hydrophobic, whereas the same loop is negatively charged in Kcc4 (Fig. 2 D). Remarkably, mutations of the hydrophobic residues F704 and F705 to aspartic acid (D) abolished Cdr2-Cter clustering (Fig. 3, A and B). Moreover, the interaction between differentially tagged Cdr2-Cter^{FF*} mutants was strongly impaired in pull-down experiments (Fig. 3 C). Intriguingly,

Published June 30, 2014

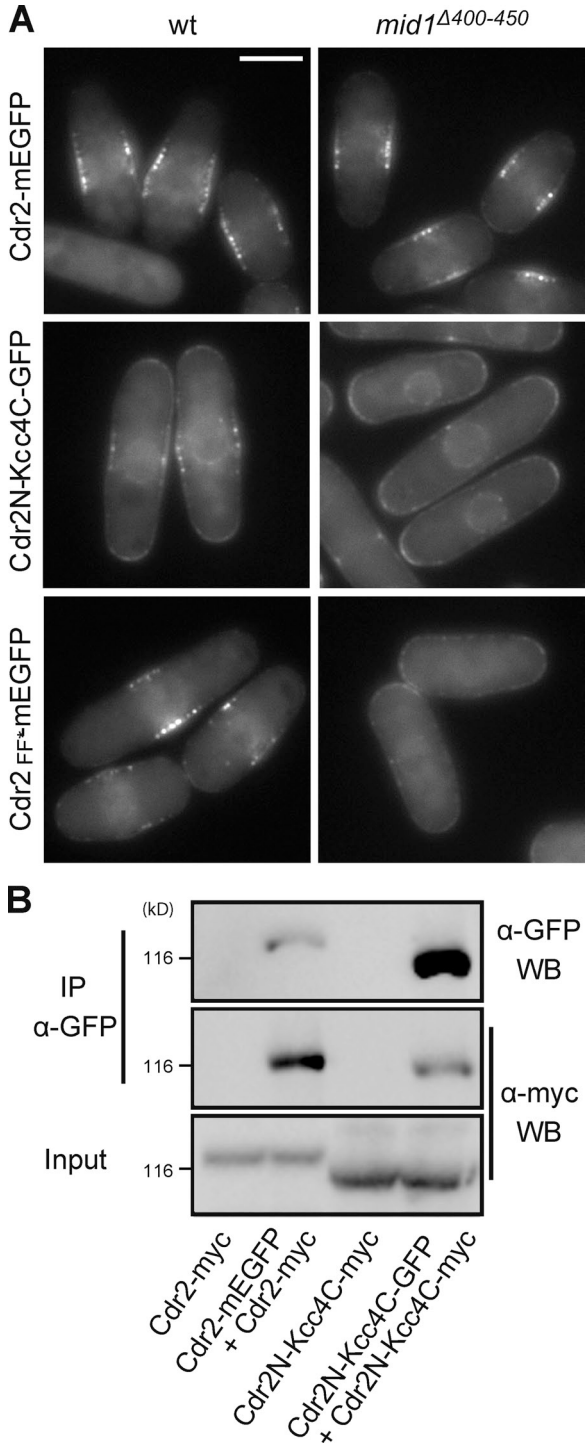

Figure 4. **Mid1 contributes to Cdr2 N-terminal clustering.** (A) Medial plane epifluorescence images of Cdr2-mEGFP, Cdr2N-Kcc4C–GFP chimera, and Cdr2^{FF*}-mEGFP in wild-type (wt) cells and *mid1*$^{\Delta 400–450}$ mutant deficient for Mid1 interaction with Cdr2. Bar, 5 µm. (B) Coimmunoprecipitation assays between mEGFP- and myc$_{12}$-tagged Cdr2 or GFP- and myc$_{12}$-tagged Cdr2N-Kcc4C. Immunoprecipitations were performed with anti-GFP mAb. Inputs and immunoprecipitation (IP) samples were probed with anti-GFP and anti-myc mAbs. Molecular masses are indicated. WB, Western blot.

Cdr2-Cter^{FF*} was distributed evenly along the cortex (Fig. 3 A), suggesting that clustering is necessary to maintain a differential distribution between the medial cortex and the cell tips.

To confirm the specificity of these mutations on Cdr2-Cter oligomerization properties, Cdr2-Cter^{FF*} was next compared with Cdr2-Cter$^{\Delta bsc}$, which lacks the basic region preceding the KA-1 domain. In this case, Cdr2-Cter$^{\Delta bsc}$ still formed clusters (Fig. 3, A and B), and similar to wild-type Cdr2-Cter, differentially tagged Cdr2-Cter$^{\Delta bsc}$ mutants interacted in pull-down experiments (Fig. 3 C).

Finally, we introduced the mutations of hydrophobic residues of the β4–β5 loop in full-length Cdr2 (Cdr2^{FF*}). This led to fewer medial nodes and a small pool of the mutant protein at the cell tips (Figs. 3 E, 4 A, and S2 A). The mutations also resulted in a slightly increased cytoplasmic pool and increased dynamics on the cortex, consistent with a reduced clustering ability (Fig. 3, D and E). Combination of these mutations with mutations in the basic region preceding the KA-1 domain enhanced Cdr2 detachment from the cortex and confirmed that these two regions of Cdr2 cooperate to establish Cdr2 nodes at the cell medial cortex (Fig. S2 A).

In summary, Cdr2 KA-1 is not only essential for membrane binding but also plays a role in Cdr2 clustering. Based on our homology modeling, this specific property of Cdr2 KA-1 compared with Kcc4 KA-1 depends on a hydrophobic loop positioned on the surface opposite to that binding the membrane.

Because the mutations of F704 and F705 disrupted clustering of Cdr2-Cter much more than it disrupted clustering of full-length Cdr2 (Fig. 3, A and E), we examined whether Cdr2 sequences N terminal to Cdr2-Cter also contribute to Cdr2 node assembly. We constructed a Cdr2N-Kcc4C chimera, in which Cdr2-Cter (residues 591–775) was replaced by Kcc4-Cter (residues 917–1,037), to target the Cdr2 N terminus to the cortex. Whereas the Kcc4-Cter does not assemble into nodes on its own (Fig. 2 A), the Cdr2N-Kcc4C chimera formed nodes, though with much lower efficiency compared with full-length Cdr2 (Fig. 4 A). Differentially tagged Cdr2N-Kcc4C chimeras could also interact with one another in immunoprecipitation experiments, although the interactions were weaker than with full-length Cdr2 molecules (Fig. 4 B). Thus, Cdr2 N-terminal regions exhibit clustering properties in addition to the C-terminal KA-1 domain.

We showed previously that Cdr2 associates with the anillin-like protein Mid1 in medial nodes (Almonacid et al., 2009; Moseley et al., 2009). Moreover, Mid1 can self-interact, and a fragment that includes the Cdr2 interaction domain was recently reported to form octamers in vitro (Celton-Morizur et al., 2004; Almonacid et al., 2009; Saha and Pollard, 2012). We thus tested whether Mid1 could play a role in Cdr2 clustering and found that the clustering of Cdr2 N terminus was dependent on interactions with Mid1, as Cdr2N-Kcc4C nodes were abolished in *mid1*$^{\Delta 400–450}$, which lacks the Cdr2 interaction site (Fig. 4 A). Node assembly was also largely disrupted when *mid1*$^{\Delta 400–450}$ was combined with the Cdr2^{FF*} mutation, which was deficient for KA-1–dependent clustering (Fig. 4 A). In contrast, a control experiment showed that the clustering of Cdr2-Cter was maintained in the *mid1*$^{\Delta 400–450}$ mutant (Fig. S2 B). We conclude that Cdr2 clustering relies on self-interactions of the C-terminal KA-1 domain and on N-terminal interactions with Mid1.

Published June 30, 2014

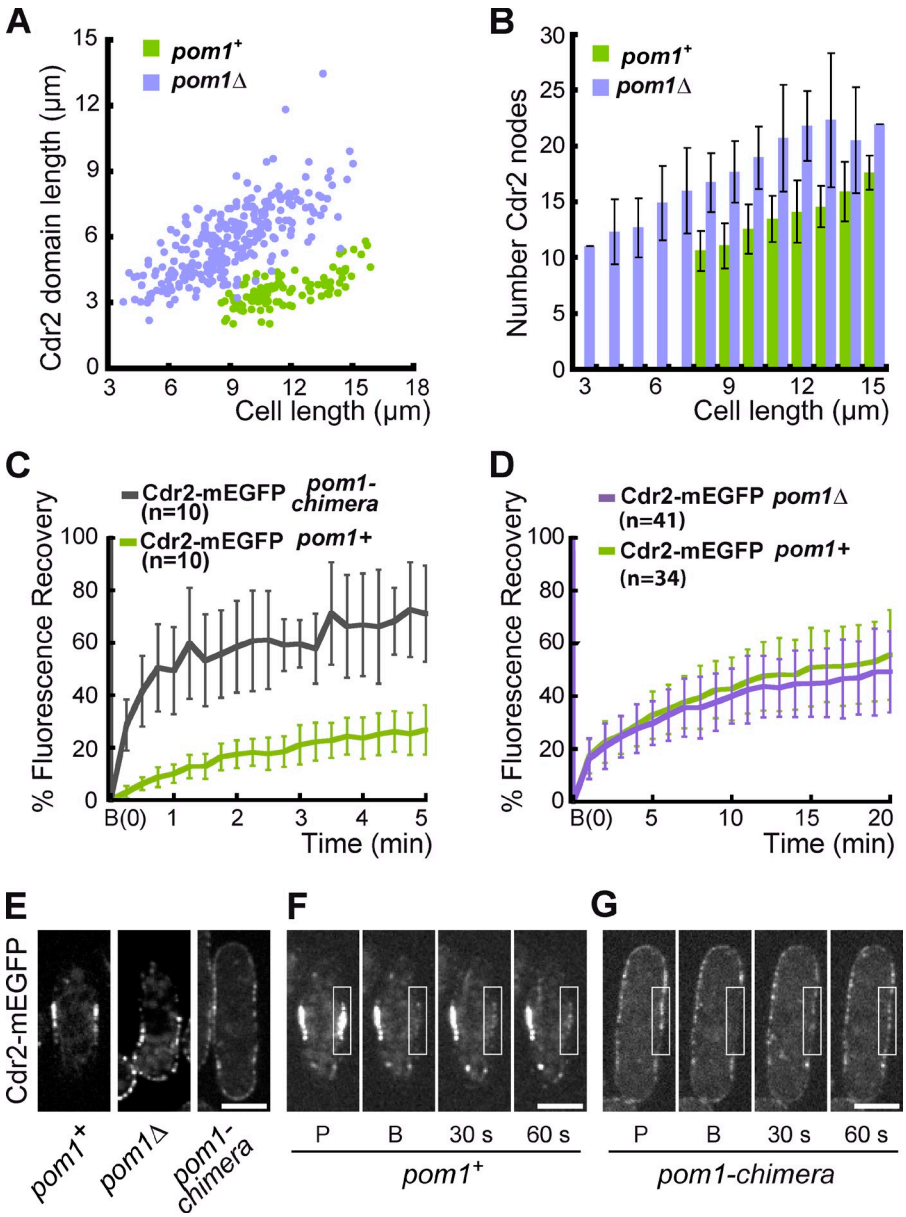

Figure 5. **Pom1 controls Cdr2 node assembly by modulation of its dynamic exchange on the cortex.** (A) Length of the domain occupied by Cdr2-mEGFP nodes in the medial focal plane relative to cell length in wild-type (n = 105) and *pom1Δ* cells (n = 296). (B) Number of Cdr2-mEGFP nodes in the medial focal plane relative to cell length in wild-type and *pom1Δ* cells. (C and D) Mean FRAP of Cdr2-mEGFP on the medial cortex in wild-type cells and cells expressing Pom1-chimera (C) or in wild-type and *pom1Δ* cells (D). Error bars show SDs. Cdr2 $t_{1/2}$ in C: *pom1*$^+$ $t_{1/2}$ > 90 s; *pom1-chimera* = 15 s < $t_{1/2}$ < 30 s. Cdr2 $t_{1/2}$ in D: *pom1*$^+$ $t_{1/2}$ = ∼3 min; *pom1Δ* $t_{1/2}$ = ∼3 min. (E) Cdr2-GFP localization in wild-type and *pom1Δ* cells and in wild-type cells expressing Pom1-chimera. (F) Example of FRAP of Cdr2-mEGFP on the medial cortex in a wild-type cell. The bleached regions are boxed. (G) Example of FRAP of Cdr2-mEGFP on the medial cortex in a cell expressing Pom1-chimera. The bleached regions are boxed. P, prebleach; B, bleach. Bars, 4 μm.

Pom1 modulates Cdr2 dynamics on the cortex

We next analyzed how Pom1 controls Cdr2 node distribution on the cortex by comparing quantitatively the number and distribution of nodes in wild-type cells and in *pom1Δ* cells, which grow in a monopolar fashion with Cdr2 nodes invading the nongrowing cell tip (Bähler and Pringle, 1998; Martin and Berthelot-Grosjean, 2009; Moseley et al., 2009). We found that in *pom1Δ* cells, the Cdr2 domain spanned approximately two thirds of the cell length compared with approximately one third in wild-type, from cell birth through cell division (Fig. 5, A and E). Moreover, the number of nodes was significantly increased in *pom1Δ* cells (Fig. 5, B and E). This suggested that Pom1 may prevent node assembly in cell tip regions, where it is most concentrated, in parallel with cell growth, which restricts nodes from growing regions independently of Pom1 by an unknown mechanism.

We reasoned that to prevent node assembly, Pom1 may regulate Cdr2 interaction with the cortex through modulation of Cdr2 membrane binding and/or clustering. To test this, we expressed a Pom1C-Mid1C chimera (called Pom1-chimera hereafter) in which the Mid1 C-terminal amphipathic helix targets Pom1 kinase domain to the medial cortex independently of Cdr2 (Celton-Morizur et al., 2004; Almonacid et al., 2009). This construct was previously shown to induce Cdr2 redistribution on the cortex and to delay mitotic entry (Moseley et al., 2009), demonstrating that the Pom1 kinase domain is active. We found that the expression of Pom1-chimera strongly increased Cdr2 dynamics on the cortex as measured by FRAP (Fig. 5, C, F, and G).

In contrast, we did not detect significant changes in Cdr2 exchange rate on the medial cortex upon *pom1* deletion (Fig. 5 D). In these cells, Cdr2 was detected in the nongrowing cell tip region as expected (Fig. 5 E; Martin, 2009; Moseley et al., 2009).

Published June 30, 2014

We measured slightly faster exchange rates at nongrowing cell tips than on the medial cortex (Fig. S3 A).

We conclude that Pom1 may normally restrict Cdr2 nodes to the medial cortex by increasing Cdr2 dynamic exchange at the cell tips, thereby restricting node assembly to the cell middle where Cdr2 can associate more stably with the cortex. Pom1-independent factors could also contribute to a minor extent to the differential regulation of Cdr2 exchange on the cortex between nongrowing cell tips and the cell middle.

Pom1 down-regulates Cdr2 clustering by modulation of Cdr2–Mid1 interaction

To increase Cdr2 turnover on the cortex, Pom1 could reduce Cdr2 affinity for the plasma membrane or down-regulate its clustering properties. Using the Pom1-chimera, we first tested a possible effect of Pom1 on Cdr2 N-terminal clustering. Strikingly, neither Cdr2N-Kcc4C chimera nor $Cdr2^{FF*}$ mutant formed nodes in the presence of Pom1-chimera and redistributed toward the cell tips in a smoother pattern (Figs. 6 A and S3 C). We also found after careful quantification that Pom1-chimera reduced by ∼50% the level of Mid1 coimmunoprecipitation with Cdr2N-Kcc4C (Fig. 6 B) and by ∼25% the degree of colocalization between Cdr2 and Mid1 nodes at the medial cortex (Fig. 6 C). In contrast, the degree of colocalization between Cdr2 and Mid1 nodes remained similar upon *pom1* deletion (Fig. S3 B). Together, these results indicate that Pom1 negatively regulates the Mid1-dependent clustering of Cdr2 N terminus.

It has been shown that Cdr2 association with Mid1 partially depends on Cdr2 kinase activity (Almonacid et al., 2009; Moseley et al., 2009). Accordingly, we found that disrupting Cdr2 kinase activity by introduction of a kinase-dead mutation (E177A referred to as $Cdr2^{KD}$; Morrell et al., 2004) abolished Cdr2N-Kcc4C node formation (Fig. 6 A). A similar result was obtained with the $Cdr2^{FF*}$ mutant (Fig. S3 C). Disrupting Cdr2 kinase activity also reduced both Mid1 coimmunoprecipitation with Cdr2N-Kcc4C chimera and the degree of Mid1 colocalization with Cdr2 cortical nodes, mimicking the effect of Pom1 (Fig. 6, B and C).

In contrast, as reported previously (Almonacid et al., 2009; Moseley et al., 2009), $Cdr2^{KD}$ mutation alone or in combination with $mid1^{\Delta 400–450}$ was neither sufficient to affect node formation by full-length Cdr2 nor to mimic Pom1-chimera effect on its dynamic exchange on the cortex (Figs. 6 A and S3, D and E). Thus, inhibiting the Mid1-dependent clustering of the Cdr2 N terminus is not sufficient to recapitulate Pom1 effect on Cdr2. This indicates that Pom1 may regulate additional properties of Cdr2 besides Mid1-dependent clustering.

Pom1 phosphorylates Cdr2 C-terminal basic motif

We thus tested whether Pom1 also acts on the Cdr2 C terminus (Fig. 7, A and B). Analysis of Cdr2-Cter distribution on the cortex revealed that it was largely excluded from both cell tips in most wild-type cells but enriched at one or both cell tips in the majority of *pom1Δ* cells, reminiscent of the localization of full-length Cdr2 in *pom1Δ* cells (Martin and Berthelot-Grosjean, 2009; Moseley et al., 2009). In addition, Cdr2-Cter was more enriched at both tips upon expression of Pom1-chimera. Cdr2-Cter clustering was not affected in these conditions. Finally, deletion of the Cdr2-Cter basic motif also induced a redistribution of Cdr2-Cter toward the cell tips, suggesting that this basic motif could be a Pom1 target.

Proteomic analysis of phosphopeptides from Cdr2-mEGFP immunoprecipitated from wild-type cells revealed four sites phosphorylated in vivo within the Cdr2-Cter basic motif (S604, S607, S616, and S618; Figs. 7 C and S4 A). In addition, recombinant GST-Pom1 phosphorylated a maltose-binding protein (MBP)–Cdr2 fragment comprising the Cdr2-Cter basic motif (aa 518–620) in vitro (Figs. 7 D and S4 B). Mutation of these four sites to nonphosphorylatable residues ($Cdr2^{bsc\text{-}4A}$) reduced ^{32}P incorporation (shorter Cdr2 fragments within this region could not be tested as substrates as they were unfortunately unstable or insoluble; Figs. 7 D and S4 B). These results suggest that the four sites represent some of the Pom1 phosphosites on Cdr2, although other as-yet-unidentified phosphosites may also be targeted by Pom1 in vitro.

Substitution of S618 by aspartic acid, alanine, or arginine in Cdr2 expressed from its endogenous locus led to cell elongation at division in all cases (unpublished data), suggesting that mutations of this amino acid may unfold the region and alter Cdr2 interaction with the cortex nonspecifically, precluding a functional interpretation of these results. We therefore produced a triple substitution of serines 604, 607, and 616 to aspartic acid (Cdr2-$Cter^{bsc\text{-}3D}$ and $Cdr2^{bsc\text{-}3D}$ mutants) to mimic phosphorylation or to alanine to inhibit phosphorylation (Cdr2-$Cter^{bsc\text{-}3A}$ and $Cdr2^{bsc\text{-}3A}$ mutants). These mutations affected the cortical distribution of Cdr2-Cter only mildly (Figs. 7 E and 8 A). Nevertheless, intensity measurements revealed that Cdr2-$Cter^{bsc\text{-}3D}$ and Cdr2-$Cter^{bsc\text{-}3A}$ were less concentrated in the medial region compared with cell tips (Fig. 7 F). The localization of full-length $Cdr2^{bsc\text{-}3D}$ and $Cdr2^{bsc\text{-}3A}$ mutants was largely similar to wild-type Cdr2, although a small pool of these mutants could be detected at the cell tips in ∼40% of cells (Fig. S5 A). FRAP analysis also revealed faster exchange rates for $Cdr2^{bsc\text{-}3D}$ on the cortex compared with wild-type Cdr2 (Fig. S5 B). In contrast, exchange rates were slightly slower when serines 604, 607, and 616 were converted to basic residues ($Cdr2^{bsc\text{-}3R}$; Fig. S5 B). This confirms that the basic region establishes electrostatic interactions with acidic phospholipids of the plasma membrane that can be negatively modulated by negative charges mimicking phosphorylation or artificially enhanced by addition of basic residues. Collectively, these results suggest that the Cdr2 C-terminal basic motif, adjacent to the KA-1 domain, is a direct target of Pom1 to modulate Cdr2 affinity for acidic phospholipids of the plasma membrane.

Combining mutations in the basic regions with inhibition of N-terminal clustering recapitulates Pom1 regulation

As described thus far, the two relatively mild effects of Pom1 on Cdr2 (effect on clustering mediated through the Cdr2 N-terminal region and effect on membrane binding involving the C-terminal basic motif adjacent to the KA-1 domain) are

Published June 30, 2014

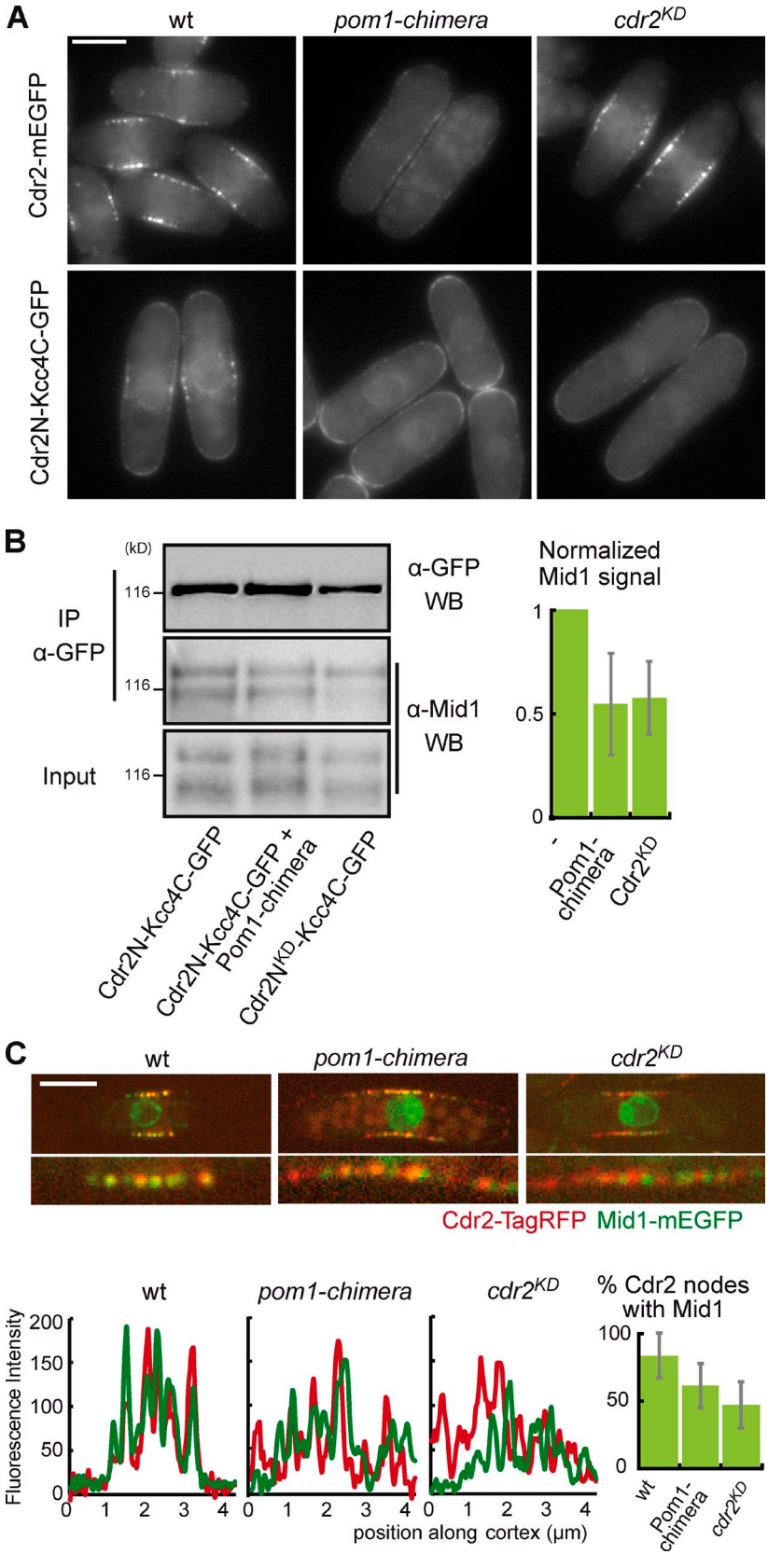

Figure 6. **Cdr2 N-terminal clustering is under the control of Pom1 and Cdr2 kinase activity.** (A) Medial plane epifluorescence images of Cdr2-mEGFP and Cdr2N-Kcc4C–GFP chimera in wild-type (wt) cells or cells expressing Pom1-chimera or carrying a Cdr2 kinase-dead mutation (KD; E177A). (B) Coimmunoprecipitation assays between Cdr2N-Kcc4C–GFP and Mid1 in wild-type cells and cells expressing the Pom1-chimera or $Cdr2N^{KD}$-Kcc4–GFP and Mid1. Immunoprecipitations were performed with anti-GFP mAb. Inputs and immunoprecipitation (IP) samples were probed with anti-GFP mAb and anti-Mid1 affinity-purified antibody. Mean normalized Mid1 coimmunoprecipitation signals from four independent experiments are shown on the right. Error bars show SDs. Molecular masses are indicated. (C, top) Medial plane confocal images of Mid1-mEGFP and Cdr2-TagRFP in wild-type cells (left) and cells expressing the Pom1-chimera (center) or of Mid1-mEGFP and $Cdr2^{KD}$-TagRFP (right). (bottom) Mid1-mEGFP and Cdr2-TagRFP intensity along the medial cortex in the same cell. (bottom right) Mean percentage of Cdr2-TagRFP nodes containing Mid1-mEGFP in individual cells. Error bars show SDs ($n \geq 25$ cells). WB, Western blot. Bars, 5 µm.

individually insufficient to promote Cdr2 node disassembly. We thus tested next whether their combination could recapitulate Pom1 inhibition of node assembly. To do so, we produced a double *cdr2*$^{bsc\text{-}3D}$ *mid1*$^{\Delta 400\text{–}450}$ mutant to mimic the dual regulation performed by Pom1. In this context, Cdr2 node assembly was strongly affected specifically in the number of nodes (Fig. 8, A and B).

Published June 30, 2014

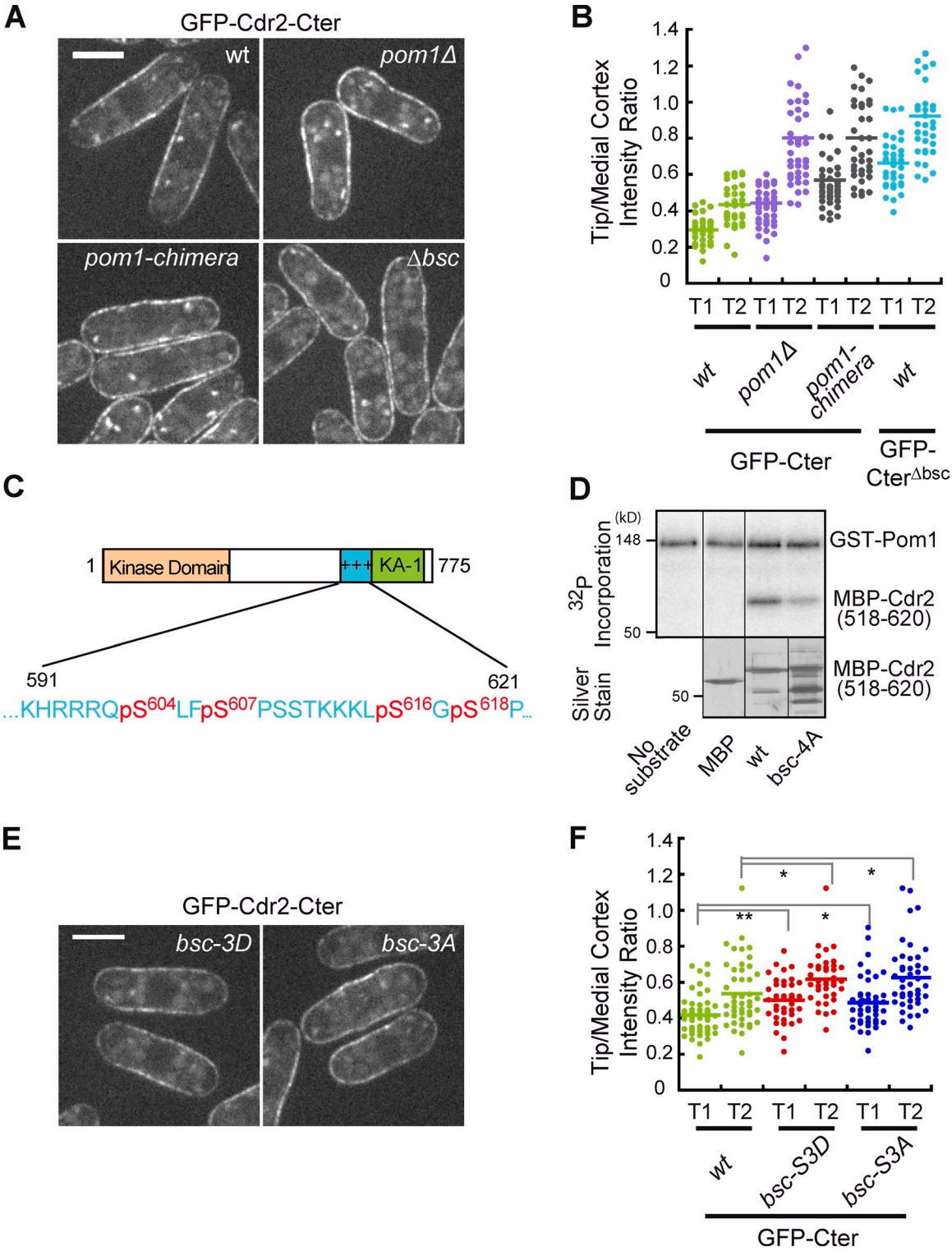

Figure 7. **Pom1 phosphorylates the Cdr2 C-terminal basic domain to modulate Cdr2 association with membranes.** (A) Localization of GFP–Cdr2-Cter in wild-type (wt) and *pom1Δ* cells or in cells expressing the Pom1-chimera and of GFP–Cdr2-Cter$^{\Delta bsc}$ in wild-type cells. (B) GFP–Cdr2-Cter fluorescence intensity ratio between the cell tip and the medial cortex in strains shown in A: Cdr2-Cter (n = 31), Cdr2-Cter *pom1Δ* (n = 39), Cdr2-Cter Pom1-chimera (n = 37), and Cdr2-Cter$^{\Delta bsc}$ (n = 34) from two experiments. T1, tip of lowest intensity; T2, tip of highest intensity. Horizontal bars are means. (C) Scheme highlighting the sequence of Cdr2 basic domain and residues found to be phosphorylated in vivo (red). (D) In vitro kinase assay of GST-Pom1 on MBP-Cdr2(518–620) with the indicated mutations. (top) Phosphorimager detection of ^{32}P incorporation. (bottom) Silver-stained gel. The top band represents Pom1 autophosphorylation. Molecular masses are indicated. Black bars indicate that intervening lanes have been spliced out. (E) Localization of GFP–Cdr2-Cter$^{bsc\text{-}3D}$ (S604D, S607D, and S616D) or GFP–Cdr2-Cter$^{bsc\text{-}3A}$ (S604A, S607A, and S616A). (F) GFP–Cdr2-Cter fluorescence intensity ratio between the cell tip and the medial cortex in strains shown in E. Cdr2-Cter (n = 45), Cter$^{bsc\text{-}3D}$ (n = 39), and Cter$^{bsc\text{-}3A}$ (n = 44) from one experiment representative of two repeats. Horizontal bars are means. Gray bars represent t tests: *, $P < 5 \times 10^{-2}$; **, $P < 5 \times 10^{-3}$. Bars, 5 µm.

Published June 30, 2014

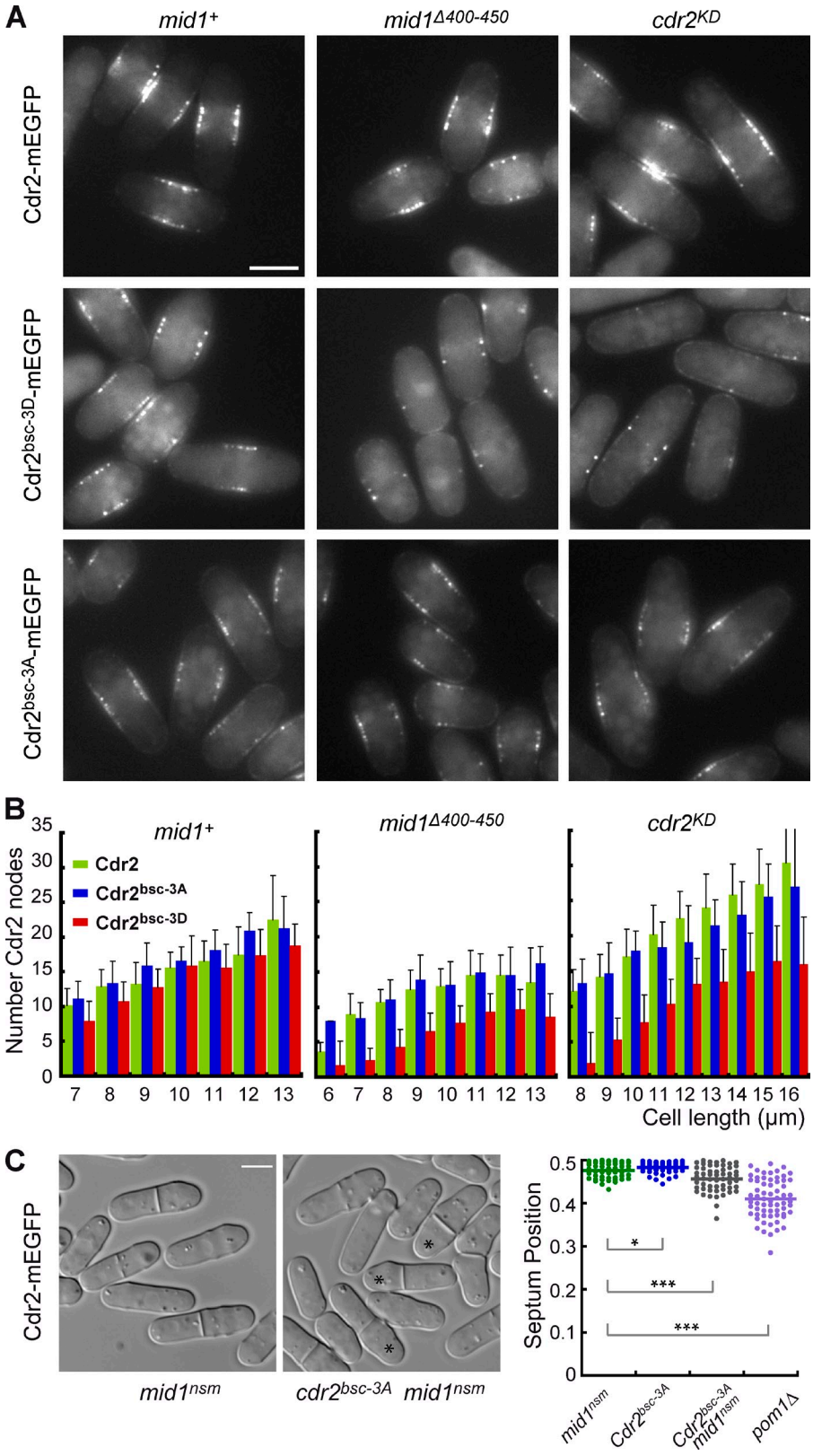

Figure 8. **Combined modulations of membrane anchoring and N-terminal clustering strongly affect Cdr2 node assembly.** (A) Localization of mEGFP-tagged Cdr2, Cdr2$^{bsc\text{-}3D}$, and Cdr2$^{bsc\text{-}3A}$ in wild-type and *mid1*$^{\Delta 400\text{–}450}$ cells or when Cdr2 also carries the E177A kinase-dead mutation (KD). (B) Number of nodes in the medial focal plane relative to cell length in similar cells as in A. Error bars show SDs. (C) Differential interference contrast images of *mid1*^{nsm} or *cdr2*$^{bsc\text{-}3A}$ *mid1*^{nsm} cells (left) and asymmetric positioning of the division plane measured as a ratio between the distance between septum and closest cell tip over total cell length in *mid1*^{nsm} (n = 48), *cdr2*$^{bsc\text{-}3A}$ (n = 53), *cdr2*$^{bsc\text{-}3A}$ *mid1*^{nsm} (n = 53), and *pom1Δ* cells (n = 64) from one experiment out of three repeats (right). Asterisks show cells with an asymmetrically positioned septum. Horizontal bars are means. *t* tests: *, $P < 5 \times 10^{-2}$; ***, $P < 10^{-5}$. Bars, 5 µm.

In contrast, combining *cdr2*$^{bsc\text{-}3A}$ with *mid1*$^{\Delta 400\text{–}450}$ did not impair node assembly. Similar results were obtained when *cdr2*$^{bsc\text{-}3D}$ or *cdr2*$^{bsc\text{-}3A}$ was combined to the *cdr2*^{KD} mutation (Fig. 8, A and B).

We finally tested whether the *cdr2*$^{bsc\text{-}3A}$ mutant presented functional defects in division plane positioning similar to *pom1Δ* cells. Because Cdr2-dependent positioning of Mid1 is corrected by Mid1 export from the nucleus at mitotic entry (Almonacid et al., 2009), we combined the *cdr2*$^{bsc\text{-}3A}$ mutation with the *mid1*^{nsm} mutation preventing Mid1 shuttling in the nucleus (Almonacid et al., 2009). Measuring septum position, we

Published June 30, 2014

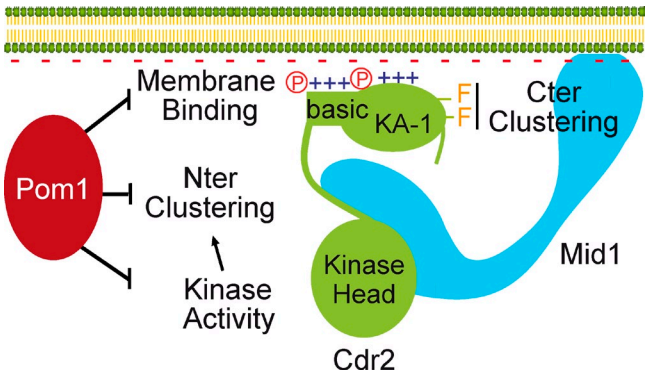

Figure 9. **Model for Pom1-dependent regulation of Cdr2 node assembly to restrict Cdr2 nodes to the medial cortex.** Cdr2 binding to the plasma membrane depends on Cdr2 C terminus containing a KA-1 domain and basic motif that establish electrostatic interaction with acidic phospholipids such as phosphatidylserine. Cdr2 clustering relies on a unique property of Cdr2 KA-1 domain involving the hydrophobic loop (FF) as well as on Cdr2 N-terminal region in a Mid1-dependent manner. Pom1 prevents node assembly at the cell tips by phosphorylating the basic motif, reducing its affinity for lipids, and by modulating the Cdr2 N-terminal interaction with Mid1 involved in clustering. This second regulation exerted by Pom1 could result indirectly from an inhibition of Cdr2 activity by Pom1 kinase. Cter, C terminus; P, phosphorylation.

found that the double mutant divided more asymmetrically than either single mutant (Fig. 8 C), although the degree of asymmetry was less pronounced than in *pom1Δ* cells. We conclude that the *cdr2*$^{bsc\text{-}3A}$ mutant exhibits some Pom1-resistant properties for division plane positioning.

We conclude that Pom1 restricts Cdr2 node assembly to the cell middle by a dual modulation of its clustering and affinity for membrane lipids. The fact that similar effects are elicited by preventing Mid1-dependent clustering of the Cdr2 N terminus and by inhibition of Cdr2 kinase activity suggests that the Pom1 effect on Cdr2 clustering could possibly rely on the down-regulation of Cdr2 kinase activity (Fig. 9).

Discussion

Fission yeast assembles its cytokinetic contractile ring in two major steps: first, by recruitment of ring components on precursors nodes in a medial region of the cortex and second, by compaction of mature nodes into a tight and well-centered ring. Such a mechanism may be evolutionarily conserved because two genetically independent steps of assembly have also been described in *Caenorhabditis elegans* (Lewellyn et al., 2010).

A key feature of this assembly mechanism is that precursor nodes are heterooligomeric assemblies of membrane-binding proteins. A detailed description of the composition and number of molecules present in these nodes before and after their mitotic maturation has been obtained (Wu et al., 2003; Wu and Pollard, 2005; Almonacid et al., 2009; Laporte et al., 2011; Akamatsu et al., 2014), and node motion studies combined with mathematical modeling have revealed that transient actomyosin-dependent attraction forces between nodes can promote their compaction into a functional ring with the contribution of F-actin–bundling proteins (Vavylonis et al., 2008; Ojkic et al., 2011; Laporte et al., 2012). In particular, modeling highlighted that the total number of cortical nodes and the width of their distribution must remain in a narrow range for an efficient assembly process.

Cdr2 has been shown to be the major node scaffolding component, which initiates node assembly during interphase (Almonacid et al., 2009; Moseley et al., 2009). Nevertheless, how Cdr2 controls node assembly and how the Pom1 gradients function to influence node distribution and limit node number and node spreading to a narrow region of the medial cortex have remained unclear. In this work, we established some of the key molecular properties by which Cdr2 can assemble into cortical nodes and deciphered molecular mechanisms of Pom1-dependent control of node assembly.

Cdr2 membrane binding and clustering properties drive node assembly

Cdr2 ability to assemble into cortical nodes relies on (a) Cdr2 membrane binding properties and (b) Cdr2 propensity to assemble into clusters of molecules. Membrane binding is ensured primarily by a C-terminal lipid-binding KA-1 domain, which functions similarly to Kcc4 KA-1 (Moravcevic et al., 2010) and may bind to phosphatidylserine, an abundant acidic phospholipid of the inner leaflet of the plasma membrane. Accordingly, using a model of Cdr2 KA-1 based on Kcc4 crystal structure, we could show that Cdr2 KA-1 possesses several likely surface-exposed basic residues that are required for Cdr2 targeting to the cortex and likely establish electrostatic interactions with acidic phospholipids of the plasma membrane.

Membrane binding of Cdr2 is reinforced by a basic motif that lies a few residues before Cdr2 KA-1 along the Cdr2 sequence. This motif is of particular interest, as we found that it constitutes a modulator of Cdr2 membrane binding affinity that is targeted by Pom1 kinase (see Pom1 controls Cdr2 node assembly and distribution in Discussion).

Cdr2 clustering depends on a dual mechanism. It involves primarily Cdr2 KA-1. This additional and unique clustering property of Cdr2 KA-1 compared with previously characterized KA-1s (Moravcevic et al., 2010) involves the hydrophobic β4–β5 loop containing two phenylalanine residues, not conserved in Kcc4 KA-1 and located opposite to the putative membrane binding surface in the Cdr2 KA-1 model. Additional work will be necessary to establish how this loop confers oligomerization properties to Cdr2 KA-1. Interestingly, this feature of Cdr2 KA-1 may be shared with other fission yeast species and other filamentous fungi because the β4–β5 loop of Cdr2 orthologues in *Schizosaccharomyces japonicus* or *Aspergillus nidulans* also contain hydrophobic residues (unpublished data).

The second mechanism of clustering depends on Cdr2 N-terminal region and requires Mid1. This result was unexpected because Cdr2 was previously shown to assemble into nodes in the absence of Mid1 or when Mid1 cannot interact with Cdr2 (Mid1$^{\Delta 400\text{–}450}$ mutant; Almonacid et al., 2009; Moseley et al., 2009). Indeed, the Mid1–Cdr2 interaction was shown to recruit Mid1 to Cdr2 nodes (Almonacid et al., 2009; Moseley et al., 2009). Our results now show it also contributes to reinforcing these nodes through Cdr2 clustering, in addition to the KA-1 domain. Clustering mediated by a partner protein is reminiscent

Published June 30, 2014

of the reported septin-dependent clustering of Kcc4 at the bud neck (Moravcevic et al., 2010) and may rely on Mid1 oligomerization properties (Celton-Morizur et al., 2004; Saha and Pollard, 2012). Because the Mid1–Cdr2 interaction is reinforced by Blt1 and Gef2 (Guzman-Vendrell et al., 2013), these components of medial cortical nodes may also contribute to Cdr2 clustering. Similar to the nonessential membrane-binding basic motif, Mid1-dependent Cdr2 clustering is of particular physiological interest because it can be modulated by Pom1 (see next section).

Pom1 controls Cdr2 node assembly and distribution

Our work shows that Pom1 controls the distribution of Cdr2 nodes in two distinct ways: modulation of Cdr2 membrane binding and modulation of Mid1-dependent clustering (Fig. 9). Mass spectrometry (MS) and in vitro phosphorylation experiments identified four phosphorylation sites within the Cdr2 basic motif. Among them, S604 but not the others, matches the R-$(X)_{1–3}$-S/T-P/V/L DYRK2 consensus. However, we note that DYRK kinases phosphosites are sometimes loosely related to the consensus, in particular Pom1 autophosphorylation sites identified from bacterially expressed Pom1 (Campbell and Proud, 2002; Aranda et al., 2011; Hachet et al., 2011). Functional analysis showed Pom1-dependent phosphorylations on the C-terminal basic motif increase slightly Cdr2 exchange rate on the cortex without important effect on node assembly on their own.

Whereas Pom1 does not appear to modulate the unique clustering properties of Cdr2 KA-1 domain, we found that it acts on Mid1-dependent clustering of Cdr2 in addition to the aforementioned modulation of Cdr2 affinity for lipids. Thus, Mid1, which represents the physiological target of Pom1-dependent spatial regulation of Cdr2 nodes for division plane positioning, appears to contribute to its own spatial regulation rather than bind passively to Cdr2 nodes prepositioned in the cell middle by Pom1.

It is interesting that the effect of Pom1 on Mid1-dependent clustering of Cdr2 can be mimicked by a down-regulation of Cdr2 kinase activity, which has been shown to modulate Mid1 recruitment to Cdr2 nodes (Almonacid et al., 2009; Moseley et al., 2009). It is thus possible that Pom1 controls Cdr2 clustering by modulating its activity. One recently proposed mechanism by which Pom1 may inhibit Cdr2 activity, without a noted effect on Cdr2 node localization or assembly, involves Pom1-dependent phosphorylation of the short C-terminal tail of Cdr2 after the KA-1 domain (Bhatia et al., 2014; Deng et al., 2014). This phosphorylation was shown to antagonize the phosphorylation of Cdr2 T loop by the calcium/calmodulin-dependent protein kinase kinase Ssp1, necessary for the activation of Cdr2 (Deng et al., 2014).

However, this C-terminal tail phosphorylated by Pom1 is absent in the Cdr2N-Kcc4–KA-1 chimera used to establish that Pom1 regulates Mid1-dependent clustering of Cdr2. Future experiments will thus be necessary to address if and how Pom1 controls Cdr2 kinase activity independently of the C-terminal tail.

Although neither of the two additional effects exerted by Pom1 on Cdr2 that we describe here is sufficient on its own, we show that mimicking them simultaneously strongly reduces the efficiency of node assembly. We propose that, by combining two mild effects on membrane binding and clustering, Pom1 renders Cdr2 node assembly less favorable at the cell tips compared with other regions of the cortex, leading to accumulation of stable nodes at the cell middle. The Cdr2 clustering properties may further reinforce this localization by increasing the avidity of Cdr2 molecules for regions with established nodes compared with Cdr2-free regions of the cortex, thus creating a positive feedback focusing the concentration of Cdr2 on the medial cortex.

We note that the assembly of Cdr2 nodes is not fully abolished upon modulation of Cdr2 membrane binding and Mid1-dependent clustering. It is thus possible that Pom1 has additional effects on Cdr2, through as-yet-unidentified phosphorylation sites or on Cdr2 partners within medial cortical nodes (e.g., Mid1, Blt1, or Gef2) to further inhibit node assembly.

Additional factors are also likely to contribute to Cdr2 node spatial restriction to the cell middle besides Pom1. Indeed, it is well established that in the absence of Pom1, Cdr2 node distribution depends on the cell's growth pattern (Martin and Berthelot-Grosjean, 2009; Moseley et al., 2009), though how growth prevents Cdr2 node assembly remains elusive. Possible factors contributing to Cdr2 exclusion from growing cell tips include lipid microdomains, sterol-rich microdomains in particular because they are enriched at cell tips (Wachtler et al., 2003), and filipin treatment was shown to disrupt Cdr2 nodes (Morrell et al., 2004). Interestingly, in *pom1Δ* cells, the Cdr2 domain, which spans approximately two thirds of the cell length, keeps enlarging with cell length, indicating that Cdr2 domain enlargement with cell size may be largely driven by cell extension. This growth pattern–dependent control may thus further reinforce Cdr2 medial localization, in addition to the Pom1-dependent mechanisms described here.

Finally, the presence of Cdr2 at the cell cortex is important not only for division plane positioning but also for the timing of cell division (Morrell et al., 2004; Martin and Berthelot-Grosjean, 2009; Moseley et al., 2009). Accordingly, we found that mutants with important cortex anchoring defects displayed a longer cell size at division, suggesting that minimum amounts of cortical Cdr2 are necessary for timely entry in mitosis. Nevertheless, we also showed recently that a 50% reduction of Cdr2 amounts does not modify cell length at division in diploids, whereas mild overexpression of Cdr2 in haploids strongly advances mitosis only if *pom1* is deleted (Bhatia et al., 2014). These data indicate that mitotic commitment is fairly robust to alterations in Cdr2 levels when Cdr2 activity is under Pom1 control. Thus, the Pom1-dependent regulation of Cdr2 node assembly described here may primarily serve as an input for division plane placement, whereas the timing of cell division is modulated by Pom1-dependent regulation of Cdr2 kinase activity (Bhatia et al., 2014; Deng et al., 2014).

In conclusion, our work provides a first mechanistic model for how Pom1 gradients can delineate the medial region of the cell where Cdr2 cooperates with Mid1 to assemble precursor nodes for the actomyosin ring to determine the position of the division plane accurately and robustly and favor the production of equally sized daughter cells. This model may be conceptually relevant to spatial regulatory events involving membrane-based gradients during cell polarity establishment in other eukaryotes.

Published June 30, 2014

Materials and methods

Yeast genetics and culture

Standard *S. pombe* media and genetic manipulations were used (Moreno et al., 1991). All strains used in the study were isogenic to wild-type 972 and are described in Table S1. Strains from genetic crosses were selected by random spore germination or tetrad dissection and replica in plates with appropriate supplements or drugs. Transformations were performed using the lithium acetate–DMSO method as previously described (Bähler et al., 1998).

Production of mutant and tagged strains

Cdr2 deletion strain, a gift from J. Moseley (Geisel School of Medicine, Dartmouth College, Hanover, NH; Moseley et al., 2009) was produced by homologous recombination using the pFa6a-NatMX6 plasmid (Hentges et al., 2005) as previously described (Bähler et al., 1998). All *cdr2* mutant alleles were integrated at the *cdr2* endogenous locus, except those cloned in pJK148- or pJK210-derived plasmids, as detailed in Table S1. These constructs were, respectively, integrated at the *leu1* and *ura4* locus under the control of their own promoter unless stated otherwise.

Mutants of Cdr2 KA-1 domain, basic region, or Cdr2 kinase-dead mutant ($Cdr2^{KD}$ carrying the E177A substitution) were produced by site-directed mutagenesis of pSR3, a pBluescript plasmid carrying Cdr2 ORF, or by double PCR. Most mutants were then subcloned between BamHI and PacI sites in pSR34 (Guzman-Vendrell et al., 2013), a pFA6a-mEGFP-KanMX6–derived plasmid carrying *cdr2* promoter and terminator for integration at *cdr2* locus in a *cdr2Δ::NatMX6* strain, in replacement of the NatMX6 cassette by homologous recombination. Plasmids were digested with NotI before transformation.

Cdr2N-Kcc4C and $Cdr2N^{KD}$-Kcc4C chimeras containing Cdr2 residues 1–590 and Kcc4 residues 917–1,037, C-terminally tagged with GFP, were inserted between BamHI and AscI sites of pSR34. Plasmids were digested with SpeI before transformation.

The sequence encoding Cdr2-Cter (residues 591–747) N-terminally tagged with GFP, carrying or not carrying mutations (*FF**, *Δbsc*, *bsc-3D*, and *bsc-3A*), was cloned between PacI and AscI sites in pSR25. GFP–Kcc4-Cter (residues 893–1,037) was cloned in pSR25 between BamHI and AscI sites.

$Cdr2^{hlx1*}$, $Cdr2^{hlx2*}$, and $Cdr2^{hlx3*}$ mutants C-terminally tagged with GFP were cloned between XhoI and SalI sites in a pJK148-derived plasmid (Keeney and Boeke, 1994) containing *cdr2* promoter and *nmt1* terminator. Plasmids were digested with NruI before transformation.

Cdr2, Cdr2-Cter, $Cdr2\text{-}Cter^{\Delta bsc}$, $Cdr2\text{-}Cter^{FF*}$, and Kcc4-Cter were also cloned between XhoI and NotI sites in a pJK148 plasmid containing the *cdr2* promoter, a C-terminal myc_{12} tag derived from pINV-myc (Iacovoni et al., 1999), and the *nmt1* terminator. Plasmids were digested with NruI before transformation.

Cdr2N-Kcc4C chimera was subcloned between XhoI and NotI sites in a pJK210-derived plasmid (Keeney and Boeke, 1994) containing the *cdr2* promoter, a C-terminal myc_{12} tag, and the *nmt1* terminator. This plasmid was digested with StuI before transformation.

To produce a Cdr2-TagRFP strain, TagRFP was amplified by PCR from pTagRFP-N (Evrogen) and cloned between PacI and AscI sites in pFa6a-GFP::NatMX6 (Hentges et al., 2005) in replacement of GFP to obtain the pFa6a-TagRFP::NatMX6. This plasmid was used to integrate TagRFP in the C terminus of Cdr2 at the endogenous locus (Bähler et al., 1998).

Pom1-chimera, previously referred to as PMT (plasma membrane targeting)-Pom1C chimera, was expressed from a construct derived from the pAM18 plasmid, integrated at *leu1* locus by homologous recombination (Moseley et al., 2009). This construct encodes amino acids 500–920 of Mid1 in fusion with amino acids 591–1,087 of Pom1 and mCherry under the control of *mid1* promoter. To produce Pom1-chimera–HA_3, the mCherry tag from pAM18 (Moseley et al., 2009) was exchanged by an HA_3 epitope. The plasmid was digested with NruI and integrated at the *leu1* locus in AP3788, a *mid1-mEGFP::kanMX6 cdr2-TagRFP::natMX6* strain.

For strong overexpression, Cdr2-Cter, $Cdr2\text{-}Cter^{\Delta bsc}$, $Cdr2\text{-}Cter^{FF*}$, and Kcc4-Cter were cloned between NdeI and NotI in pREP1-GST, a gift from P. Perez (Instituto de Biología Funcional y Genómica, Salamanca, Spain). For bacterial expression, Cdr2-Cter was cloned between BamHI and NotI sites in pGEX6p-1 (GE Healthcare).

Various serine to alanine mutants in Cdr2 phosphosites on the basic domain were produced by site-directed mutagenesis of pSM788, a pBluescript plasmid carrying Cdr2 ORF and 5′UTR and 3′UTR regions between NotI and SalI. Cdr2 fragments amplified from pSM788 or the mutant plasmids were cloned between BamHI and XhoI sites in pGEX-4T-1 or NotI and XhoI in a pMAL–tobacco etch virus (TEV) vector, respectively, and used for recombinant protein production and kinase assays. A list of the plasmids used in the study can be found in Table S2.

Microscopy and image analysis

For epifluorescence images shown in Figs. 1 C, S1 A, 2 A, S2, 3 A, S3 C, 4 A, 6 A, and 8 A or transmission images in Fig. 8 C and spinning-disc confocal images shown in Figs. S3 (B and D), 5 (E–G), 6 C, and 7 (A and E), cells were grown at 25°C in YE5S. Epifluorescence images were taken on an upright microscope (DMRXA2; Leica) controlled with MetaMorph software 7.7.8 (Molecular Devices) and equipped with a 100×, 1.4 NA oil immersion Plan Apochromat objective and a charge-coupled device camera (CoolSNAP HQ2; Photometrics) with an exposure time of 2 s. Confocal images were taken on a fully motorized inverted microscope (Eclipse Ti-E; Nikon) controlled with MetaMorph software 7.7.8 and equipped with the Perfect Focus System (Nikon) to maintain the focus, a 100×, 1.45 NA Plan Apochromat oil immersion objective, a piezo stage (Mad City Labs), a confocal unit (CSUX1; Yokogawa Corporation of America), a charge-coupled device camera (CoolSNAP HQ2), and a laser bench (Errol) with a 491–561-nm diode laser (100 mW each; Cobolt). Exposure time for GFP, mCherry, or tdTomato was 2 s (or 0.5 s for Fig. S3 D). Laser power was 30% (back pupil of the objective: 1.9 mW), binning was set at 2, and electronic gain was set to 3. All images were scaled similarly to their respective control using MetaMorph software 7.7.8.

FRAP experiments of Figs. 1 D, 3 D, 5 (C and D), S3 E, and S5 were performed on the Eclipse spinning-disk setup. The FRAP module was controlled by iLas software (Roper Scientific) integrated to MetaMorph software 7.7.8. Medial cortex regions of 30 × 5 pixels (3.7 µm long) were bleached for 200 ms at 100% laser power (back pupil of the objective: 8.1 mW), after five image acquisitions at 1-s intervals. Postbleach images were acquired every 60 s (or 15 s in Fig. 5 C) over a 20-min period and were exposed over 0.5 s at 30% laser power, binning at 2, and electronic gain at 3 (for a 5-min period in Fig. 5 C). For fluorescence recovery analysis, images were first registered with the ImageJ plugin StackReg (National Institutes of Health) and analyzed with MetaMorph software 7.7.8. In brief, bleaching correction was performed by calculating the mean Cdr2 intensity decay along the acquisition of at least five nonbleached cells. Bleaching correction was individually applied to each bleached region. Bleaching recovery curves were then normalized with the first point after bleaching corresponding to 0% and the first point before bleaching corresponding to 100% and averaged. $t_{1/2}$'s were estimated graphically as the time point after bleaching when half-maximum recovery was reached. Maximum recovery was defined as the mean intensity of the last four data points.

Analysis of Cdr2-mEGFP domain length and node number shown in Fig. 5 (A and B) was performed on epifluorescence images. In Figs. 6 C and S3 B, Mid1-mEGFP and Cdr2-TagRFP cortical fluorescence intensity was measured along a 100-pixel-long line on the medial cortex with the Linescan tool of MetaMorph software 7.7.8 (3 pixel width) on single medial focal planes. The percentage of Cdr2 nodes containing Mid1 was derived from these line scans as the percentage of Cdr2 peaks that coincided with a Mid1 peak. Similarly, for Fig. 7 (B and F), fluorescence intensity of GFP–Cdr2-Cter was recorded along a 40-pixel-long line on the cell tip and medial cortex, and the intensity ratio was calculated after background deduction.

For cell length measurements, cells were grown at 30°C in Edinburgh minimal medium supplemented with uracil, adenine, and leucine. Cell length measurements were made with MetaMorph software on differential interference contrast images of septating cells taken on the DMRXA2 microscope described previously in this section. In all comparisons made, strains with identical auxotrophies were used.

Cdr2 KA-1 3D homology modeling

3D homology modeling was performed according to Šali and Blundell (1993) using the Modeler 9.0 in the DS Modeling 1.7 software package (Accelrys). The model for Cdr2 KA-1 was generated by using the coordinates of Kcc4 KA-1 (Protein Data Bank accession no. 3OSM). The structural quality of the models was assessed according to the Modeler probability density functions as well as Profiles-3D analysis (DS Modeling 1.7). Out of the 10 models generated, the one with the lowest energy was selected. 3D molecular representations were obtained by using PyMOL (DeLano Scientific LLC).

Analysis of phosphorylation sites by MS

For MS analysis, Cdr2-GFP was purified from extracts of nonsynchronous cells using anti-GFP mAb (Roche) as previously described (Almonacid et al., 2011). After immunoprecipitation, proteins were submitted to SDS-PAGE

Published June 30, 2014

gels. Excised gel slices were washed, and proteins were reduced with 10 mM DTT before alkylation with 55 mM iodoacetamide. After washing and shrinking of the gel pieces with 100% acetonitrile, in-gel digestion was performed using trypsin (Sequencing Grade; Promega) overnight in 25 mM ammonium bicarbonate at 30°C. The extracted peptides were analyzed by nano–liquid chromatography-MS/MS using an UltiMate 3000 system (Dionex) coupled to a mass spectrometer (LTQ Orbitrap XL; Thermo Fisher Scientific). Samples were loaded on a C18 precolumn (300-µm inner diameter × 5 mm; Dionex) at 20 µl/min in 5% acetonitrile and 0.1% TFA. After 3 min of desalting, the precolumn was switched on line with the analytical C18 column (75-µm inner diameter × 50 cm; C18 PepMap; Dionex) equilibrated in solvent A (2% acetonitrile and 0.1% formic acid). Bound peptides were eluted using a 160-min linear gradient (from 0 to 30% [vol/vol]) of solvent B (80% acetonitrile and 0.085% formic acid) at a 150-nl/min flow rate and an oven temperature of 40°C. Data-dependent acquisition was performed on the mass spectrometer (LTQ Orbitrap XL) in the positive ion mode. Survey MS scans were acquired in the LTQ Orbitrap XL on the 400–1,200 mass per charge range with the resolution set to a value of 100,000. Each scan was recalibrated in real time by coinjecting an internal standard from ambient air into the C-trap (lock mass option). The five most intense ions per survey scan were selected for collision-induced dissociation fragmentation, and the resulting fragments were analyzed in the linear trap (LTQ Orbitrap XL). Target ions already selected for MS/MS were dynamically excluded for 30 s. Data were acquired using the Xcalibur software (version 2.2; Thermo Fisher Scientific), and the resulting spectra were then analyzed via the Mascot and the Sequest software created with Proteome Discoverer (version 1.4; Thermo Fisher Scientific) using the Swiss-Prot *Schizosaccharomyces pombe* (fission yeast) database, containing 5,089 protein sequences. Carbamidomethylation of cysteines, oxidation of methionine, protein N-terminal acetylation, and phosphorylated serine, threonine, and tyrosine were set as variable modifications for all searches. Specificity of trypsin digestion was set, and two missed cleavage site were allowed. The mass tolerances in MS and MS/MS were set to 5 ppm and 0.5 D, respectively. Phosphorylated peptides with nonphosphorylated counterparts were validated manually.

Cdr2–Cdr2 and Cdr2–Mid1 interaction experiments

Immunoprecipitations experiments shown in Figs. 4 B and 6 B were performed as previously described (Almonacid et al., 2011). In brief, 200 ml of cells grown at 1.6×10^7 cells/ml at 30°C in YE5S was resuspended in 300 µl NP-40 buffer (Celton-Morizur et al., 2004). Extracts were incubated with anti–mouse IgG magnetic beads (M-280 Dynal; Invitrogen), coupled to 6 µg anti-GFP mAB (Roche). Western blots were probed with anti-GFP mAb (1:500; Roche), antimyc mAb 9E10 (1:666; Roche), or anti-Mid1 affinity-purified Ab (1:100; Celton-Morizur et al., 2004). Secondary antibodies were coupled to peroxidase (Jackson ImmunoResearch Laboratories, Inc.). Signal quantification was performed with Image Lab 4.0.1 (Bio-Rad Laboratories). Signals of coimmunoprecipitated proteins were normalized relative to the amount of primarily immunoprecipitated protein.

For interactions between differentially tagged Cdr2-Cter shown in Figs. 2 C and 3 C, protein extracts were produced from 200 ml *cdr2Δ* cells carrying GST–Cdr2-Cter, GST–Cdr2-Cter^{FF*}, GST–Cdr2-Cter$^{\Delta bsc}$, or GST–Kcc4-Cter plasmids grown for 20 h in Edinburgh minimal medium without thiamine at 30°C to an OD of 0.8 at 600 nm to induce GST–Cdr2-Cter, GST–Cdr2-Cter^{FF*}, GST–Cdr2-Cter$^{\Delta bsc}$, or GST–Kcc4-Cter overexpression. 200 µl of extract was incubated for 2 h at 4°C with 7.5 µl of dry glutathione–Sepharose beads. Separate protein extracts were produced from 200 ml *cdr2Δ* cells expressing Cdr2-Cter–myc$_{12}$, Cdr2-Cter^{FF*}–myc$_{12}$, Cdr2-Cter$^{\Delta bsc}$–myc$_{12}$, or Kcc4-Cter–myc$_{12}$ from the *leu1* locus grown at 30°C to OD of 0.8 at 600 nm in YE5S. Beads were washed five times with NP-40 buffer. Pull-downs and supernatants were submitted to SDS-PAGE. Western blots were probed with a rabbit affinity-purified anti-GST antibody (1:100; gift from J. Dumont, Institut Jacques Monod, Paris, France), and the antimyc mAb 9E10 (1:666). Secondary antibodies were coupled to peroxidase.

Recombinant protein production and lipid-binding assay

Expression of GST–Cdr2-Cter or GST was induced in BL21 bacteria from the pGEX6p-1–derived plasmid described in Production of mutant and tagged strains. In brief, cells were grown overnight in LB (Luria–Bertani) medium supplemented with 100 µg/ml ampicillin at 37°C. 500 ml LB and 100 µg/ml ampicillin were inoculated with 12.5 ml of the saturated culture, grown for 4 h at 30°C. Protein expression was induced by the addition of 1 mM IPTG and incubation for 1 h. Bacterial pellets were resuspended in 5 ml PBS, digested with 1 mg/ml lysozyme, treated with 1 µg/ml DNase I, sonicated twice for 1 min (50% amplitude), incubated with 1% Triton X-100 in PBS buffer at 4°C, and centrifuged 15 min at 4°C at 10,000 *g*. Soluble extract was incubated with 200 µl glutathione–Sepharose beads at 50% slurry for 2 h at 4°C. Finally, beads were washed 3× with cold PBS and eluted in four steps in 100 µl elution buffer (15 mM reduced glutathione and 50 mM Tris-HCl, pH 8). Eluted proteins were incubated with lipid strips (Echelon, Inc.) following the manufacturer's protocol. Lipid strips were probed with a rabbit affinity-purified anti-GST antibody (1:100; gift from J. Dumont).

Recombinant protein production and in vitro kinase assay

Expression of GST-Cdr2 fragments from pGEX-4T-1–derived plasmids was performed as described in the "Recombinant protein production and lipid-binding assay" section. MBP-TEV-Cdr2(518–620) and MBP-TEV-Cdr2(518–620)$^{S604\text{-}607\text{-}616\text{-}618\text{-}4A}$ fragments were also induced in BL21 cells from pMAL-TEV–derived plasmid as described in the "Recombinant protein production and lipid-binding assay" section. In brief, cells were grown overnight in LB supplemented with 100 µg/ml ampicillin at 37°C. 250 ml of LB-ampicillin was inoculated with 6.25 ml of the saturated culture, grown 3 h at 37°C. Protein expression was induced by the addition of 100 µM IPTG for 5 h at 18°C. Bacterial pellets were resuspended in 10 ml of cold resuspension buffer (50 mM Tris-Cl, pH 8, 1 mM EDTA, 100 mM KCl, and PMSF), sonicated 3× for 30 s (50% amplitude), incubated with 1% Triton X-100 at 4°C, and centrifuged 15 min at 4°C at 10,000 *g*. Soluble extract was incubated with 400 µl amylose resin (New England Biolabs, Inc.) for 2 h at 4°C. Finally, beads were washed 3× with cold resuspension buffer and eluted in three steps in 100 µl elution buffer (50 mM Tris-Cl, pH 8, 1 mM EDTA, 100 mM KCl, and 10 mM maltose).

For kinase assays, recombinant GST-Pom1 or GST-Pom1^{KD} fusion proteins were expressed in BL21 cells and purified with glutathione–Sepharose 4B (GE Healthcare) columns according to the manufacturer's protocol (Hachet et al., 2011). Kinase assays were performed in 30 mM Tris, 100 mM NaCl, 10 mM $MgCl_2$, 1 mM EGTA, 10% glycerol, 1 mM DTT, 20 µM ATP, and 2 µCi [^{32}P]ATP (PerkinElmer) in a 15-µl final volume reaction. After a 30-min incubation at 30°C, the reaction was stopped by boiling in sample buffer and analyzed by SDS-PAGE. ^{32}P incorporation was detected with a phosphorimager (Typhoon FLA 7000; GE Healthcare). Silver staining was performed according to the manufacturer's protocol (Silver Stain Kit; Thermo Fisher Scientific) to check for equivalent amounts of substrates.

Online supplemental material

Fig. S1 reports additional properties of Cdr2 C-terminal domain. Fig. S2 shows the localization of the Cdr2$^{bsc*\text{-}FF*}$ mutant and of Cdr2-Cter in *mid1*$^{\Delta 400–450}$ mutant. Fig. S3 analyses the role of Pom1, Mid1, and Cdr2 kinase activity in Cdr2 node assembly. Fig. S4 defines how Pom1 phosphorylates the Cdr2 basic region. Fig. S5 analyses the dynamic exchange on the cortex of Cdr2 phosphoinhibitory or phosphomimetic mutants in the basic region. Tables S1 and S2 list strains and plasmids used in this study, respectively. Table S3 reports cell length at division in Cdr2 mutants in the C-terminal–anchoring domain. Online supplemental material is available at http://www.jcb.org/cgi/content/full/jcb.201311097/DC1.

We thank M. Riou and P. Paoletti for invaluable help to produce the Cdr2 KA-1 3D model and A. Sansaloni for help with strain construction. We also thank J. Dumont, J. Moseley, and P. Perez for strains, plasmids, and reagents and Phong Tran for critical reading of the manuscript.

This work was supported by Ligue Nationale Contre le Cancer (Programme Labellisation), Ligue Contre le Cancer Comité de Paris, and Mairie de Paris (Programme Emergence) to A. Paoletti as well as a European Research Council Starting Grant (260493) and a Swiss National Science Foundation research grant (31003A_138177) to S.G. Martin. A. Paoletti is a member of LabEx CelTisPhyBio, which is part of Idex PSL* (Initiative D'Excellence Paris Sciences et Lettres). S.A. Rincon received postdoctoral fellowships from Fundacion Ramon Areces and the Marie Curie FP7 program. M. Guzman-Vendrell received a PhD fellowship from Université Paris-Sud and Association pour la Recherche sur le Cancer.

The authors declare no competing financial interests.

Submitted: 25 November 2013
Accepted: 28 May 2014

References

Akamatsu, M., J. Berro, K.M. Pu, I.R. Tebbs, and T.D. Pollard. 2014. Cytokinetic nodes in fission yeast arise from two distinct types of nodes that merge during interphase. *J. Cell Biol.* 204:977–988. http://dx.doi.org/10.1083/jcb.201307174

Almonacid, M., and A. Paoletti. 2010. Mechanisms controlling division-plane positioning. *Semin. Cell Dev. Biol.* 21:874–880. http://dx.doi.org/10.1016/j.semcdb.2010.08.006

Almonacid, M., J.B. Moseley, J. Janvore, A. Mayeux, V. Fraisier, P. Nurse, and A. Paoletti. 2009. Spatial control of cytokinesis by Cdr2 kinase and Mid1/anillin nuclear export. *Curr. Biol.* 19:961–966. http://dx.doi.org/10.1016/j.cub.2009.04.024

Almonacid, M., S. Celton-Morizur, J.L. Jakubowski, F. Dingli, D. Loew, A. Mayeux, J.S. Chen, K.L. Gould, D.M. Clifford, and A. Paoletti. 2011. Temporal control of contractile ring assembly by Plo1 regulation of myosin II recruitment by Mid1/anillin. *Curr. Biol.* 21:473–479. http://dx.doi.org/10.1016/j.cub.2011.02.003

Alvarez-Tabarés, I., A. Grallert, J.M. Ortiz, and I.M. Hagan. 2007. *Schizosaccharomyces pombe* protein phosphatase 1 in mitosis, endocytosis and a partnership with Wsh3/Tea4 to control polarised growth. *J. Cell Sci.* 120:3589–3601. http://dx.doi.org/10.1242/jcs.007567

Aranda, S., A. Laguna, and S. de la Luna. 2011. DYRK family of protein kinases: evolutionary relationships, biochemical properties, and functional roles. *FASEB J.* 25:449–462. http://dx.doi.org/10.1096/fj.10-165837

Bähler, J., and J.R. Pringle. 1998. Pom1p, a fission yeast protein kinase that provides positional information for both polarized growth and cytokinesis. *Genes Dev.* 12:1356–1370. http://dx.doi.org/10.1101/gad.12.9.1356

Bähler, J., J.Q. Wu, M.S. Longtine, N.G. Shah, A. McKenzie III, A.B. Steever, A. Wach, P. Philippsen, and J.R. Pringle. 1998. Heterologous modules for efficient and versatile PCR-based gene targeting in *Schizosaccharomyces pombe*. *Yeast*. 14:943–951. http://dx.doi.org/10.1002/(SICI)1097-0061(199807)14:10<943::AID-YEA292>3.0.CO;2-Y

Balasubramanian, M.K., R. Srinivasan, Y. Huang, and K.H. Ng. 2012. Comparing contractile apparatus-driven cytokinesis mechanisms across kingdoms. *Cytoskeleton (Hoboken).* 69:942–956. http://dx.doi.org/10.1002/cm.21082

Bathe, M., and F. Chang. 2010. Cytokinesis and the contractile ring in fission yeast: towards a systems-level understanding. *Trends Microbiol.* 18:38–45. http://dx.doi.org/10.1016/j.tim.2009.10.002

Bhatia, P., O. Hachet, M. Hersch, S.A. Rincon, M. Berthelot-Grosjean, S. Dalessi, L. Basterra, S. Bergmann, A. Paoletti, and S.G. Martin. 2014. Distinct levels in Pom1 gradients limit Cdr2 activity and localization to time and position division. *Cell Cycle*. 13:538–552. http://dx.doi.org/10.4161/cc.27411

Bohnert, K.A., A.P. Grzegorzewska, A.H. Willet, C.W. Vander Kooi, D.R. Kovar, and K.L. Gould. 2013. SIN-dependent phosphoinhibition of formin multimerization controls fission yeast cytokinesis. *Genes Dev.* 27:2164–2177. http://dx.doi.org/10.1101/gad.224154.113

Breeding, C.S., J. Hudson, M.K. Balasubramanian, S.M. Hemmingsen, P.G. Young, and K.L. Gould. 1998. The cdr2(+) gene encodes a regulator of G2/M progression and cytokinesis in *Schizosaccharomyces pombe*. *Mol. Biol. Cell*. 9:3399–3415. http://dx.doi.org/10.1091/mbc.9.12.3399

Campbell, L.E., and C.G. Proud. 2002. Differing substrate specificities of members of the DYRK family of arginine-directed protein kinases. *FEBS Lett.* 510:31–36. http://dx.doi.org/10.1016/S0014-5793(01)03221-5

Celton-Morizur, S., N. Bordes, V. Fraisier, P.T. Tran, and A. Paoletti. 2004. C-terminal anchoring of mid1p to membranes stabilizes cytokinetic ring position in early mitosis in fission yeast. *Mol. Cell. Biol.* 24:10621–10635. http://dx.doi.org/10.1128/MCB.24.24.10621-10635.2004

Celton-Morizur, S., V. Racine, J.B. Sibarita, and A. Paoletti. 2006. Pom1 kinase links division plane position to cell polarity by regulating Mid1p cortical distribution. *J. Cell Sci.* 119:4710–4718. http://dx.doi.org/10.1242/jcs.03261

Chang, F., A. Woollard, and P. Nurse. 1996. Isolation and characterization of fission yeast mutants defective in the assembly and placement of the contractile actin ring. *J. Cell Sci.* 109:131–142.

Coleman, T.R., Z. Tang, and W.G. Dunphy. 1993. Negative regulation of the wee1 protein kinase by direct action of the nim1/cdr1 mitotic inducer. *Cell*. 72:919–929. http://dx.doi.org/10.1016/0092-8674(93)90580-J

Daga, R.R., and F. Chang. 2005. Dynamic positioning of the fission yeast cell division plane. *Proc. Natl. Acad. Sci. USA*. 102:8228–8232. http://dx.doi.org/10.1073/pnas.0409021102

Deng, L., S. Baldissard, A.N. Kettenbach, S.A. Gerber, and J.B. Moseley. 2014. Dueling kinases regulate cell size at division through the SAD kinase Cdr2. *Curr. Biol.* 24:428–433. http://dx.doi.org/10.1016/j.cub.2014.01.009

Fededa, J.P., and D.W. Gerlich. 2012. Molecular control of animal cell cytokinesis. *Nat. Cell Biol.* 14:440–447. http://dx.doi.org/10.1038/ncb2482

Fuller, B.G. 2010. Self-organization of intracellular gradients during mitosis. *Cell Div.* 5:5. http://dx.doi.org/10.1186/1747-1028-5-5

Goyal, A., M. Takaine, V. Simanis, and K. Nakano. 2011. Dividing the spoils of growth and the cell cycle: The fission yeast as a model for the study of cytokinesis. *Cytoskeleton (Hoboken).* 68:69–88. http://dx.doi.org/10.1002/cm.20500

Green, R.A., E. Paluch, and K. Oegema. 2012. Cytokinesis in animal cells. *Annu. Rev. Cell Dev. Biol.* 28:29–58. http://dx.doi.org/10.1146/annurev-cellbio-101011-155718

Guzman-Vendrell, M., S. Baldissard, M. Almonacid, A. Mayeux, A. Paoletti, and J.B. Moseley. 2013. Blt1 and Mid1 provide overlapping membrane anchors to position the division plane in fission yeast. *Mol. Cell. Biol.* 33:418–428. http://dx.doi.org/10.1128/MCB.01286-12

Hachet, O., and V. Simanis. 2008. Mid1p/anillin and the septation initiation network orchestrate contractile ring assembly for cytokinesis. *Genes Dev.* 22:3205–3216. http://dx.doi.org/10.1101/gad.1697208

Hachet, O., M. Berthelot-Grosjean, K. Kokkoris, V. Vincenzetti, J. Moosbrugger, and S.G. Martin. 2011. A phosphorylation cycle shapes gradients of the DYRK family kinase Pom1 at the plasma membrane. *Cell*. 145:1116–1128. http://dx.doi.org/10.1016/j.cell.2011.05.014

Hachet, O., F.O. Bendezú, and S.G. Martin. 2012. Fission yeast: in shape to divide. *Curr. Opin. Cell Biol.* 24:858–864. http://dx.doi.org/10.1016/j.ceb.2012.10.001

Hentges, P., B. Van Driessche, L. Tafforeau, J. Vandenhaute, and A.M. Carr. 2005. Three novel antibiotic marker cassettes for gene disruption and marker switching in *Schizosaccharomyces pombe*. *Yeast*. 22:1013–1019. http://dx.doi.org/10.1002/yea.1291

Huang, Y., H. Yan, and M.K. Balasubramanian. 2008. Assembly of normal actomyosin rings in the absence of Mid1p and cortical nodes in fission yeast. *J. Cell Biol.* 183:979–988. http://dx.doi.org/10.1083/jcb.200806151

Iacovoni, J.S., P. Russell, and F. Gaits. 1999. A new inducible protein expression system in fission yeast based on the glucose-repressed inv1 promoter. *Gene*. 232:53–58. http://dx.doi.org/10.1016/S0378-1119(99)00116-X

Jourdain, I., E.A. Brzezińska, and T. Toda. 2013. Fission yeast Nod1 is a component of cortical nodes involved in cell size control and division site placement. *PLoS ONE*. 8:e54142. http://dx.doi.org/10.1371/journal.pone.0054142

Kanoh, J., and P. Russell. 1998. The protein kinase Cdr2, related to Nim1/Cdr1 mitotic inducer, regulates the onset of mitosis in fission yeast. *Mol. Biol. Cell*. 9:3321–3334. http://dx.doi.org/10.1091/mbc.9.12.3321

Keeney, J.B., and J.D. Boeke. 1994. Efficient targeted integration at leu1-32 and ura4-294 in *Schizosaccharomyces pombe. Genetics*. 136:849–856.

Laporte, D., R. Zhao, and J.Q. Wu. 2010. Mechanisms of contractile-ring assembly in fission yeast and beyond. *Semin. Cell Dev. Biol.* 21:892–898. http://dx.doi.org/10.1016/j.semcdb.2010.08.004

Laporte, D., V.C. Coffman, I.J. Lee, and J.Q. Wu. 2011. Assembly and architecture of precursor nodes during fission yeast cytokinesis. *J. Cell Biol.* 192:1005–1021. http://dx.doi.org/10.1083/jcb.201008171

Laporte, D., N. Ojkic, D. Vavylonis, and J.Q. Wu. 2012. α-Actinin and fimbrin cooperate with myosin II to organize actomyosin bundles during contractile-ring assembly. *Mol. Biol. Cell*. 23:3094–3110. http://dx.doi.org/10.1091/mbc.E12-02-0123

Lee, I.J., V.C. Coffman, and J.Q. Wu. 2012. Contractile-ring assembly in fission yeast cytokinesis: Recent advances and new perspectives. *Cytoskeleton (Hoboken)*. 69:751–763. http://dx.doi.org/10.1002/cm.21052

Lemmon, M.A. 2008. Membrane recognition by phospholipid-binding domains. *Nat. Rev. Mol. Cell Biol.* 9:99–111. http://dx.doi.org/10.1038/nrm2328

Lewellyn, L., J. Dumont, A. Desai, and K. Oegema. 2010. Analyzing the effects of delaying aster separation on furrow formation during cytokinesis in the *Caenorhabditis elegans* embryo. *Mol. Biol. Cell*. 21:50–62. http://dx.doi.org/10.1091/mbc.E09-01-0089

Martin, S.G. 2009. Microtubule-dependent cell morphogenesis in the fission yeast. *Trends Cell Biol.* 19:447–454. http://dx.doi.org/10.1016/j.tcb.2009.06.003

Martin, S.G., and M. Berthelot-Grosjean. 2009. Polar gradients of the DYRK-family kinase Pom1 couple cell length with the cell cycle. *Nature*. 459:852–856. http://dx.doi.org/10.1038/nature08054

Moravcevic, K., J.M. Mendrola, K.R. Schmitz, Y.H. Wang, D. Slochower, P.A. Janmey, and M.A. Lemmon. 2010. Kinase associated-1 domains drive MARK/PAR1 kinases to membrane targets by binding acidic phospholipids. *Cell*. 143:966–977. http://dx.doi.org/10.1016/j.cell.2010.11.028

Moreno, S., A. Klar, and P. Nurse. 1991. Molecular genetic analysis of fission yeast *Schizosaccharomyces pombe*. *Methods Enzymol.* 194:795–823. http://dx.doi.org/10.1016/0076-6879(91)94059-L

Morrell, J.L., C.B. Nichols, and K.L. Gould. 2004. The GIN4 family kinase, Cdr2p, acts independently of septins in fission yeast. *J. Cell Sci.* 117:5293–5302. http://dx.doi.org/10.1242/jcs.01409

Moseley, J.B., A. Mayeux, A. Paoletti, and P. Nurse. 2009. A spatial gradient coordinates cell size and mitotic entry in fission yeast. *Nature*. 459:857–860. http://dx.doi.org/10.1038/nature08074

Ojkic, N., J.Q. Wu, and D. Vavylonis. 2011. Model of myosin node aggregation into a contractile ring: the effect of local alignment. *J. Phys. Condens. Matter*. 23:374103. http://dx.doi.org/10.1088/0953-8984/23/37/374103

Oliferenko, S., T.G. Chew, and M.K. Balasubramanian. 2009. Positioning cytokinesis. *Genes Dev.* 23:660–674. http://dx.doi.org/10.1101/gad.1772009

Padmanabhan, A., K. Bakka, M. Sevugan, N.I. Naqvi, V. D'souza, X. Tang, M. Mishra, and M.K. Balasubramanian. 2011. IQGAP-related Rng2p organizes cortical nodes and ensures position of cell division in fission yeast. *Curr. Biol.* 21:467–472. http://dx.doi.org/10.1016/j.cub.2011.01.059

Padte, N.N., S.G. Martin, M. Howard, and F. Chang. 2006. The cell-end factor pom1p inhibits mid1p in specification of the cell division plane in fission yeast. *Curr. Biol.* 16:2480–2487. http://dx.doi.org/10.1016/j.cub.2006.11.024

Parker, L.L., S.A. Walter, P.G. Young, and H. Piwnica-Worms. 1993. Phosphorylation and inactivation of the mitotic inhibitor Wee1 by the nim1/cdr1 kinase. *Nature*. 363:736–738. http://dx.doi.org/10.1038/363736a0

Pollard, T.D., and J.Q. Wu. 2010. Understanding cytokinesis: lessons from fission yeast. *Nat. Rev. Mol. Cell Biol.* 11:149–155. http://dx.doi.org/10.1038/nrm2834

Rincon, S.A., and A. Paoletti. 2012. Mid1/anillin and the spatial regulation of cytokinesis in fission yeast. *Cytoskeleton (Hoboken)*. 69:764–777. http://dx.doi.org/10.1002/cm.21056

Roberts-Galbraith, R.H., M.D. Ohi, B.A. Ballif, J.S. Chen, I. McLeod, W.H. McDonald, S.P. Gygi, J.R. Yates III, and K.L. Gould. 2010. Dephosphorylation of F-BAR protein Cdc15 modulates its conformation and stimulates its scaffolding activity at the cell division site. *Mol. Cell*. 39:86–99. http://dx.doi.org/10.1016/j.molcel.2010.06.012

Russell, P., and P. Nurse. 1987a. The mitotic inducer nim1+ functions in a regulatory network of protein kinase homologs controlling the initiation of mitosis. *Cell*. 49:569–576. http://dx.doi.org/10.1016/0092-8674(87)90459-4

Russell, P., and P. Nurse. 1987b. Negative regulation of mitosis by wee1+, a gene encoding a protein kinase homolog. *Cell*. 49:559–567. http://dx.doi.org/10.1016/0092-8674(87)90458-2

Saha, S., and T.D. Pollard. 2012. Characterization of structural and functional domains of the anillin-related protein Mid1p that contribute to cytokinesis in fission yeast. *Mol. Biol. Cell*. 23:3993–4007. http://dx.doi.org/10.1091/mbc.E12-07-0536

Šali, A., and T.L. Blundell. 1993. Comparative protein modelling by satisfaction of spatial restraints. *J. Mol. Biol.* 234:779–815. http://dx.doi.org/10.1006/jmbi.1993.1626

Saunders, T.E., K.Z. Pan, A. Angel, Y. Guan, J.V. Shah, M. Howard, and F. Chang. 2012. Noise reduction in the intracellular pom1p gradient by a dynamic clustering mechanism. *Dev. Cell*. 22:558–572. http://dx.doi.org/10.1016/j.devcel.2012.01.001

Sohrmann, M., C. Fankhauser, C. Brodbeck, and V. Simanis. 1996. The dmf1/mid1 gene is essential for correct positioning of the division septum in fission yeast. *Genes Dev.* 10:2707–2719. http://dx.doi.org/10.1101/gad.10.21.2707

Vavylonis, D., J.Q. Wu, S. Hao, B. O'Shaughnessy, and T.D. Pollard. 2008. Assembly mechanism of the contractile ring for cytokinesis by fission yeast. *Science*. 319:97–100. http://dx.doi.org/10.1126/science.1151086

Wachtler, V., S. Rajagopalan, and M.K. Balasubramanian. 2003. Sterol-rich plasma membrane domains in the fission yeast *Schizosaccharomyces pombe*. *J. Cell Sci.* 116:867–874. http://dx.doi.org/10.1242/jcs.00299

White, E.A., and M. Glotzer. 2012. Centralspindlin: at the heart of cytokinesis. *Cytoskeleton (Hoboken)*. 69:882–892. http://dx.doi.org/10.1002/cm.21065

Wood, E., and P. Nurse. 2013. Pom1 and cell size homeostasis in fission yeast. *Cell Cycle*. 12:3228–3236. http://dx.doi.org/10.4161/cc.26462

Wu, J.Q., and T.D. Pollard. 2005. Counting cytokinesis proteins globally and locally in fission yeast. *Science*. 310:310–314. http://dx.doi.org/10.1126/science.1113230

Wu, J.Q., J.R. Kuhn, D.R. Kovar, and T.D. Pollard. 2003. Spatial and temporal pathway for assembly and constriction of the contractile ring in fission yeast cytokinesis. *Dev. Cell*. 5:723–734. http://dx.doi.org/10.1016/S1534-5807(03)00324-1

Wu, L., and P. Russell. 1993. Nim1 kinase promotes mitosis by inactivating Wee1 tyrosine kinase. *Nature*. 363:738–741. http://dx.doi.org/10.1038/363738a0

Ye, Y., I.J. Lee, K.W. Runge, and J.Q. Wu. 2012. Roles of putative Rho-GEF Gef2 in division-site positioning and contractile-ring function in fission yeast cytokinesis. *Mol. Biol. Cell*. 23:1181–1195. http://dx.doi.org/10.1091/mbc.E11-09-0800

Zhu, Y.H., Y. Ye, Z. Wu, and J.Q. Wu. 2013. Cooperation between Rho-GEF Gef2 and its binding partner Nod1 in the regulation of fission yeast cytokinesis. *Mol. Biol. Cell*. 24:3187–3204. http://dx.doi.org/10.1091/mbc.E13-06-0301

Rincon et al., http://www.jcb.org/cgi/content/full/jcb.201311097/DC1

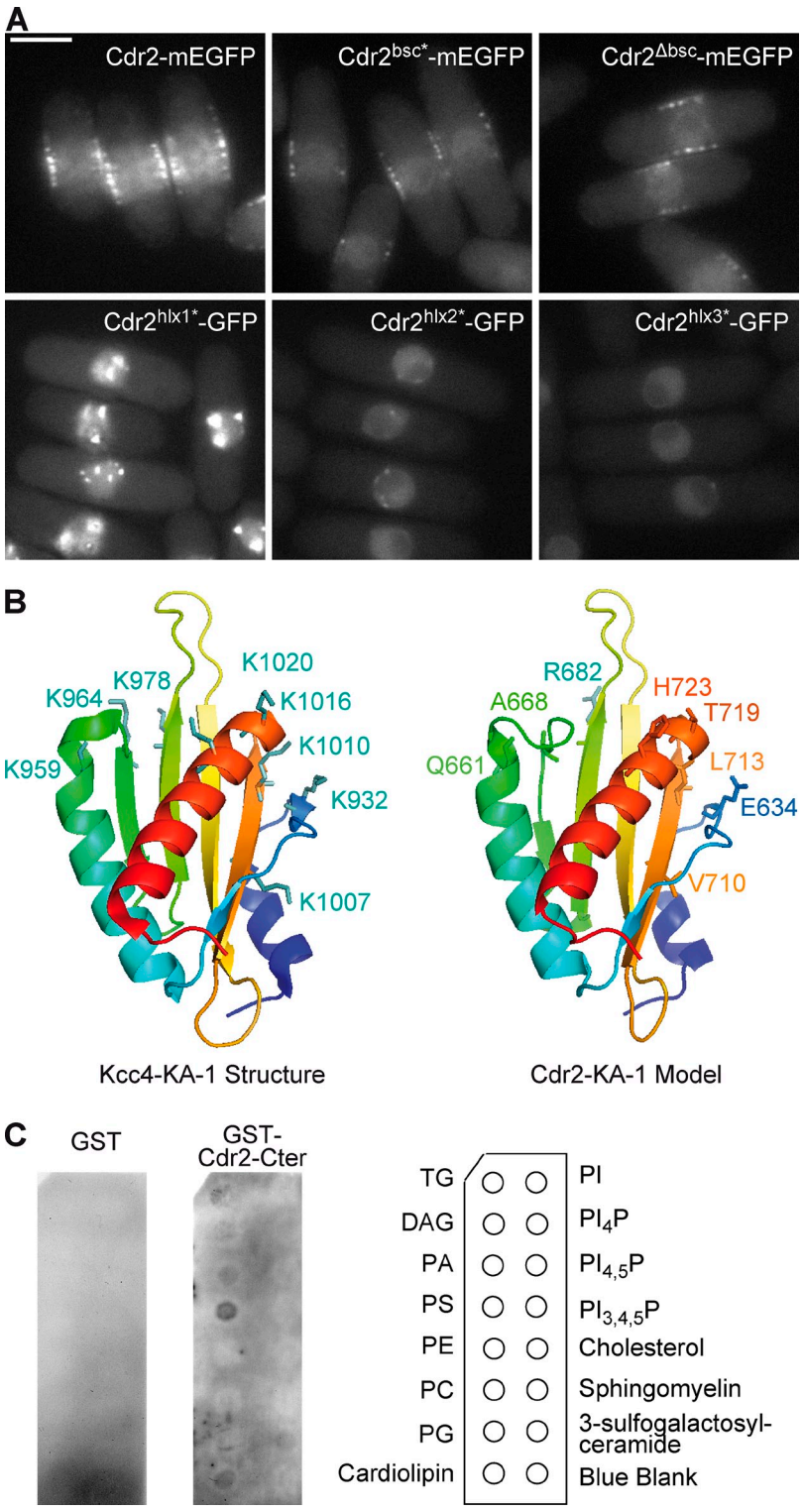

Figure S1. **Properties of Cdr2 C-terminal domain.** (A) Medial plane epifluorescence images of mEGFP-tagged Cdr2 mutated in the C-terminal basic region (Cdr2^{bsc*}), carrying a deletion of the basic region (Cdr2$^{\Delta bsc}$; deletion of residues 591–620) or mutated in the predicted helices of the KA-1 domain (Cdr2^{hlx1*}, Cdr2^{hlx2*}, and Cdr2^{hlx3*}). Bar, 5 µm. (B) Kcc4 KA-1 structure 3OST highlighting surface-exposed basic residues involved in lipid binding according to Moravcevic et al. (2010) and equivalent positions in the Cdr2 KA-1 model with nonconserved residues, except R682 that corresponds to K978 on Kcc4 KA-1. Note that the structure and model are rotated by ~180° compared with those shown in Figs. 1 B or 2 D. (C) Protein–lipid overlay assay with GST (negative control; left) and GST–Cdr2-Cter (right) purified from *Escherichia coli*. Signal was enhanced using a γ of 1.3. Dim signals are likely caused by the very low amount of soluble GST–Cdr2-Cter produced in *E. coli*. PI, phosphatidylinositol; TG, triglyceride; PA, phosphatidic acid; PS, phosphatidylserine; PE, phosphatidylethanolamine; PC, phosphatidylcholine; PG, phosphatidylglycerol.

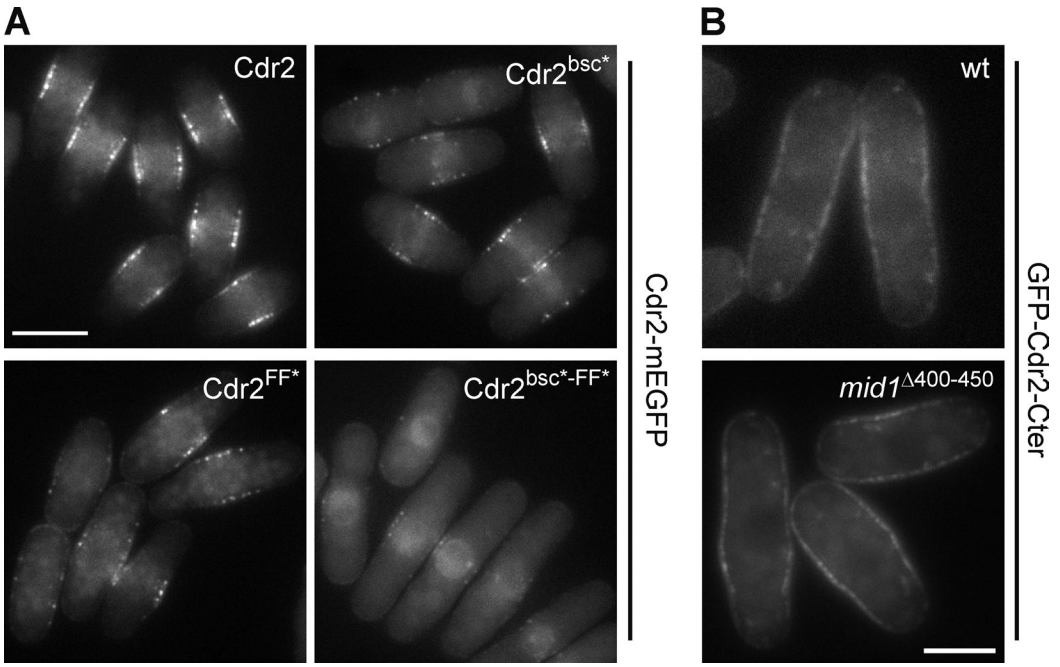

Figure S2. **Localization of the Cdr2$^{bsc*\text{-}FF*}$ mutant and of Cdr2-Cter in the *mid1*$^{\Delta 400–450}$ mutant.** (A) Medial plane epifluorescence images of Cdr2-mEGFP, Cdr2^{FF*}-mEGFP, Cdr2^{bsc*}-mEGFP, or Cdr2$^{bsc*\text{-}FF*}$-mEGFP in wild-type cells. (B) Medial plane epifluorescence images of GFP–Cdr2-Cter in wild type (wt; top) and the *mid1*$^{\Delta 400–450}$ mutant (bottom). Bars, 5 µm.

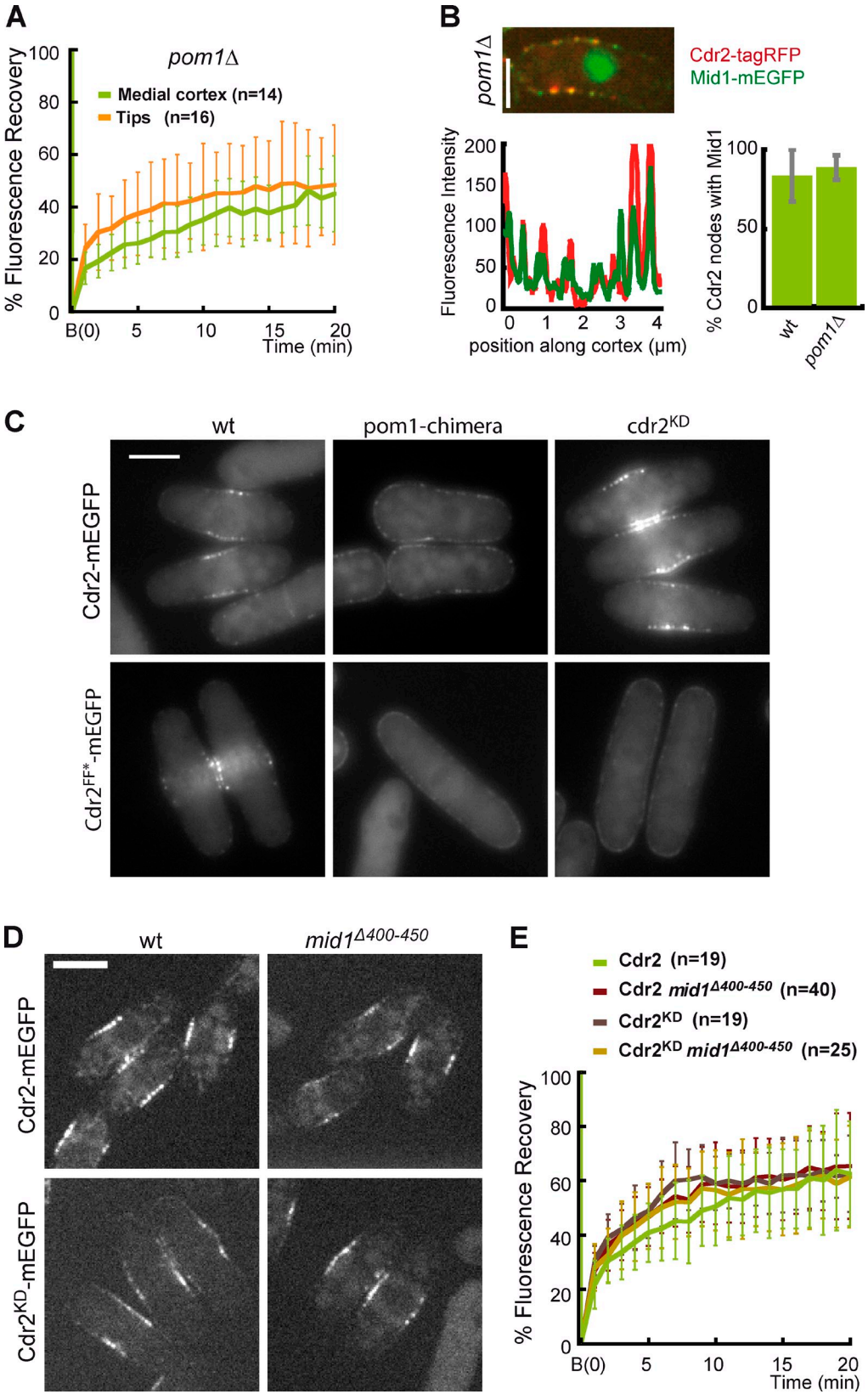

Figure S3. **Role of Pom1, Mid1, and Cdr2 kinase activity in Cdr2 node assembly.** (A) Mean FRAP of Cdr2-mEGFP on the medial cortex or at cell tips in *pom1Δ* cells. Error bars show SDs. Cdr2 $t_{1/2}$: medial cortex $t_{1/2}$ = ~3 min; tip $t_{1/2}$ < 2 min. B, bleach. (B, top) Medial plane confocal images of Mid1-mEGFP and Cdr2-TagRFP in a *pom1Δ* cell. Bar, 4 μm. (bottom) Mid1-mEGFP and Cdr2-TagRFP intensity along the cortex in the same cell. The line scan starts from top medial cortex, goes around the left cell tip, and continues until the bottom medial cortex. (bottom right) Mean percentage of Cdr2-TagRFP nodes containing Mid1-mEGFP in individual cells. Error bars show SDs (n = 25 cells). (C) Medial plane epifluorescence images of Cdr2-mEGFP and Cdr2^{FF*}-mEGFP in wild-type (wt) cells or cells expressing Pom1-chimera or carrying a Cdr2 kinase-dead mutation (E177A). (D) Medial plane confocal images of Cdr2-mEGFP or Cdr2^{KD}-mEGFP in wild-type cells or the *mid1*$^{Δ400–450}$ mutant. (E) Mean FRAP of Cdr2-mEGFP or Cdr2^{KD}-mEGFP on the medial cortex in wild-type cells or *mid1*$^{Δ400–450}$. Error bars show SDs. Cdr2 $t_{1/2}$: wild type $t_{1/2}$ = ~3 min; *mid1*$^{Δ400–450}$ $t_{1/2}$ < 2 min; Cdr2^{KD} $t_{1/2}$ < 2 min; *mid1*$^{Δ400–450}$ Cdr2^{KD} $t_{1/2}$ = ~2 min. Bar, 5 μm.

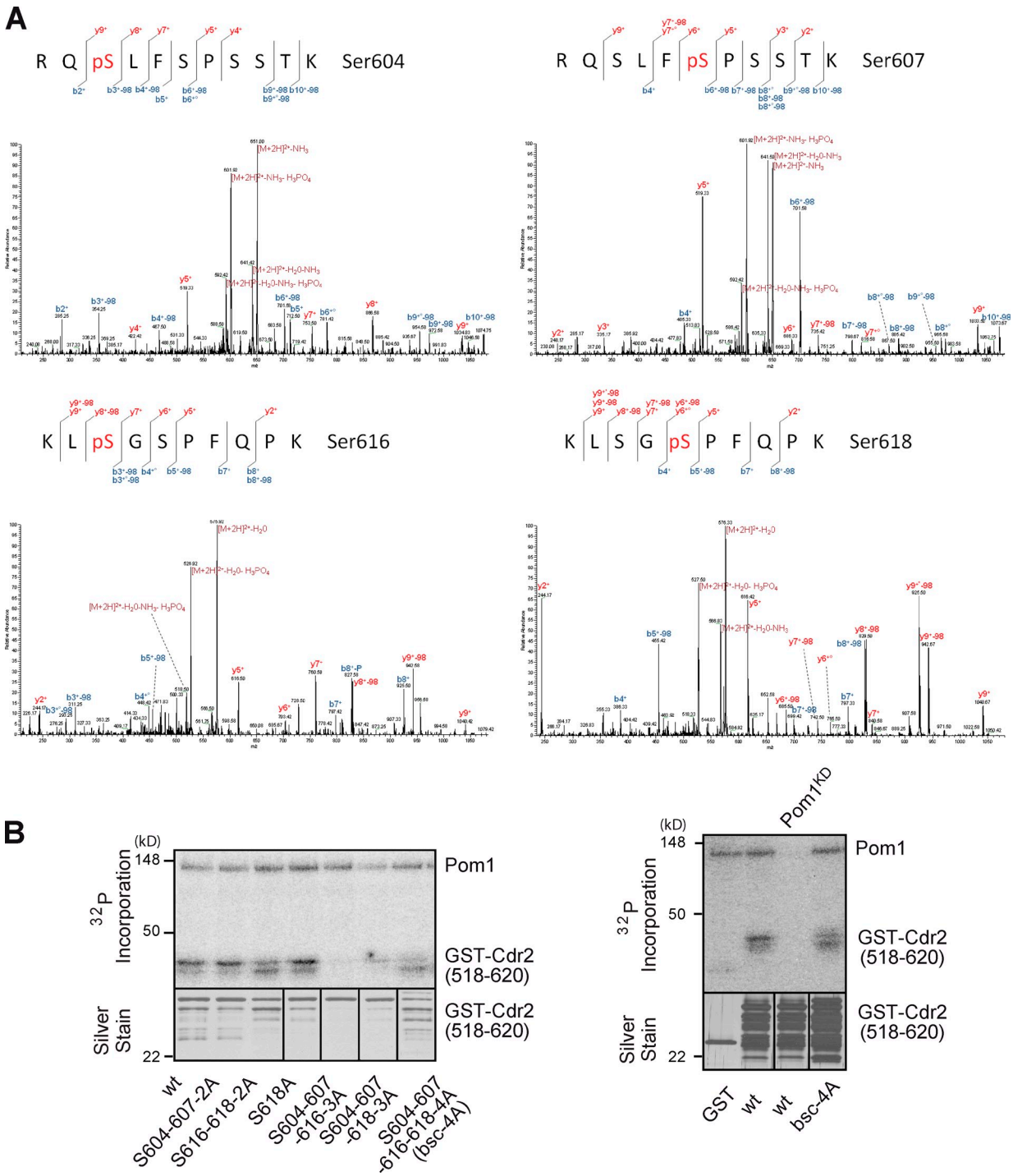

Figure S4. **Pom1 phosphorylates Cdr2 basic region.** (A) MS2 spectra of Cdr2 phosphorylated peptides within the Cdr2 basic motif. The fragmentation spectra are derived from trypsin-digested Cdr2-GFP purified with anti-GFP mAb. The phosphopeptide sequences and observed ions are indicated on top of the spectra. Singly and doubly charged b and y ions as well as ion corresponding to neutral losses of water (circles), NH_3 (asterisks), and H_3PO_4 (98 D) groups are shown. M, parent ion mass. (B and C) In vitro kinase assay of GST-Pom1 or GST-Pom1^{KD} on GST-Cdr2(518–620) with the indicated mutations. (top) Phosphorimager detection of ^{32}P incorporation. (bottom) Silver-stained gel. The second and third lanes of the silver-stained gel show the same input sample. A control using GST-Pom1^{KD} shows no ^{32}P incorporation. Molecular masses are indicated. wt, wild type. Black lines indicate that intervening lanes have been spliced out.

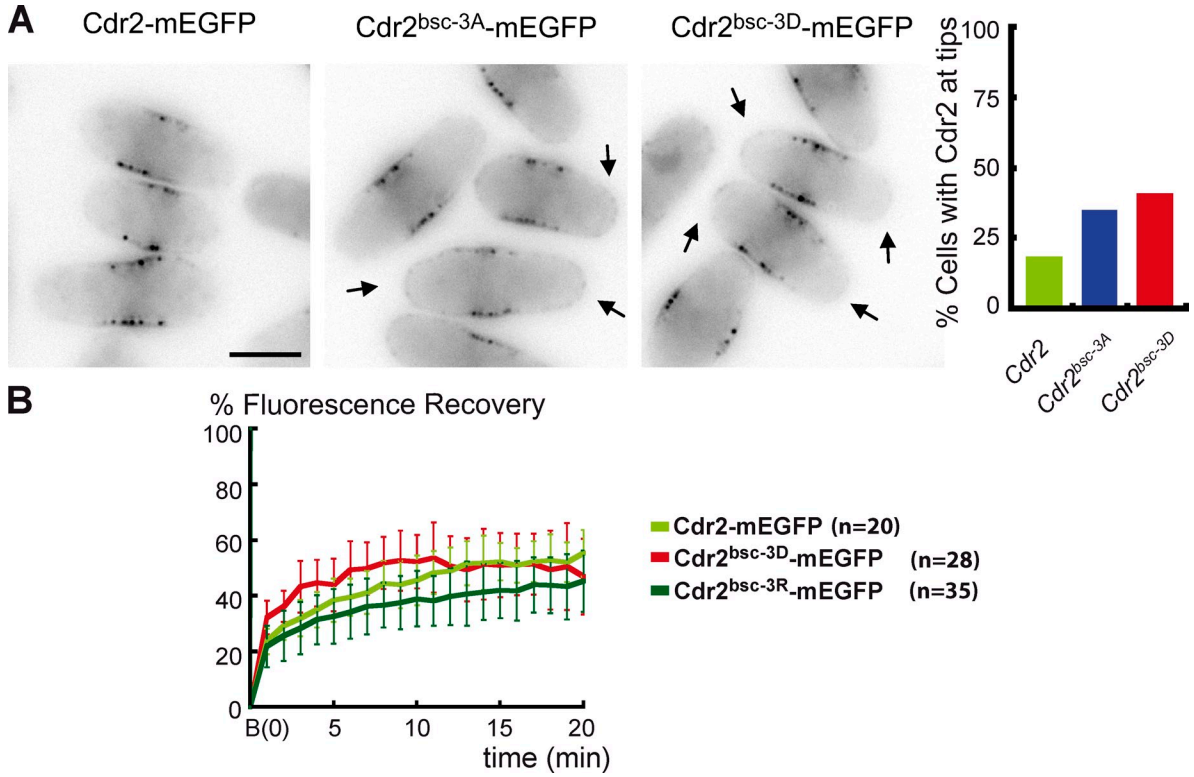

Figure S5. **Dynamic exchange on the cortex of Cdr2 phosphoinhibitory or phosphomimetic mutations in the basic region.** (A) Localization of mEGFP-tagged Cdr2, Cdr2$^{bsc\text{-}3D}$, and Cdr2$^{bsc\text{-}3A}$ at the tips of wild-type cells. Arrows show cell tip localization. Inverted black and white pictures are depicted. Bar, 5 µm. (right) Percentage of cells with Cdr2, Cdr2$^{bsc\text{-}3D}$, and Cdr2$^{bsc\text{-}3A}$ detected at cell tips. $n > 150$ cells. (B) Mean FRAP of mEGFP-tagged Cdr2, Cdr2$^{bsc\text{-}3R}$, and Cdr2$^{bsc\text{-}3D}$ on the medial cortex. Error bars shows SDs. Cdr2 $t_{1/2} > 2$ min; Cdr2$^{bsc\text{-}3R}$ $t_{1/2} > 2$ min; Cdr2$^{bsc\text{-}3D}$ $t_{1/2} < 1$ min. B, bleach.

Table S1. **List of strains used in this study**

Strain number	Genotype	Source
Fig. 1		
AP3087	h⁻ *cdr2-mEGFP:kanMX6 leu1-32*	This work
AP3568	h⁻ *cdr2^{RKRKR*}-mEGFP:kanMX6 leu1-32*	This work
AP3112	h⁻ *cdr2^{bsc*}-mEGFP:kanMX6 leu1-32*	This work
AP3418	h⁻ *cdr2^{RR*}-mEGFP:kanMX6 leu1-32*	This work
AP3548	h⁻ *cdr2$^{RR*-RKRKR*}$-mEGFP:kanMX6 leu1-32*	This work
AP3546	h⁻ *cdr2$^{bsc*-RKRKR}$-mEGFP:kanMX6 leu1-32*	This work
AP3526	h⁻ *cdr2$^{\Delta bsc}$-mEGFP:kanMX6 leu1-32*	This work
Fig. 2		
AP3081	h⁻ *GFP–cdr2-Cter:kanMX6 leu1-32 ura4-D18 ade6-M210*	This work
AP4764	h⁻ *GFP–kcc4-Cter:kanMX6 leu1-32*	This work
AP3986	h⁻ *cdr2Δ::natMX6 leu1⁺:Pcdr2-cdr2-Cter–myc$_{12}$*	This work
AP3988	h⁻ *cdr2Δ::natMX6 pREP1-GST–cdr2-Cter*	This work
AP4812	h⁻ *kcc4-Cter–myc$_{12}$:kanMX6 cdr2::natMX6 leu1-32*	This work
AP4813	h⁻ *cdr2Δ::natMX6 pREP1-GST–kcc4-Cter leu1-32*	This work
AP2804	h⁻ *cdr2::natMX6 leu1-32*	Laboratory stock
Fig. 3		
AP3081	h⁻ *GFP–cdr2-Cter:kanMX6 leu1-32 ura4-D18 ade6-M210*	This work
AP3555	h⁻ *GFP–cdr2-Cter^{FF*}:kanMX6 leu1-32*	This work
AP3503	h⁻ *GFP–cdr2-Cter$^{\Delta bsc}$:kanMX6 leu1-32*	This work
AP3986	h⁻ *cdr2Δ::natMX6 leu1⁺:Pcdr2-cdr2-Cter–myc$_{12}$*	This work
AP3987	h⁻ *cdr2Δ::natMX6 leu1⁺:Pcdr2-cdr2-Cter^{FF*}–myc$_{12}$*	This work
AP3988	h⁻ *cdr2Δ::natMX6 pREP1-GST–cdr2-Cter*	This work
AP3989	h⁻ *cdr2Δ::natMX6 pREP1-GST–cdr2-Cter^{FF*}*	This work
AP4744	h⁻ *cdr2Δ::natMX6 leu1⁺:Pcdr2-cdr2-Cter$^{\Delta bsc}$–myc$_{12}$*	This work
AP4814	h⁻ *cdr2Δ::natMX6 pREP1-GST-Cter$^{\Delta bsc}$ leu1-32*	This work
AP3087	h⁻ *cdr2-mEGFP:kanMX6 leu1-32*	This work
AP3428	h⁻ *cdr2^{FF*}-mEGFP:kanMX6 leu1-32 ura4-D18 ade6⁻*	This work
Fig. 4		
AP3087	h⁻ *cdr2-mEGFP:kanMX6 leu1-32*	This work
AP3724	h⁻ *cdr2-mEGFP:kanMX6 mid1Δ::ura4⁺ leu1⁺:Pmid1-mid1$^{\Delta 400–450}$*	This work
AP3736	h⁻ *cdr2N-kcc4C–GFP:kanMX6 leu1-32*	This work
AP3959	h⁻ *cdr2N-kcc4C–GFP:kanMX6 mid1Δ::ura4⁺ leu1⁺:Pmid1-mid1$^{\Delta 400–450}$ ade6⁻*	This work
AP3428	h⁻ *cdr2^{FF*}-mEGFP:kanMX6 leu1-32 ura4-D18 ade6⁻*	This work
AP3976	h⁺ *cdr2^{FF*}-mEGFP:kanMX6 mid1Δ::ura4⁺ leu1⁺:Pmid1-mid1$^{\Delta 400–450}$ ura4-D18 ade6⁻*	This work
AP4227	h⁺ *leu1⁺:Pcdr2-cdr2-myc$_{12}$ ura4-D18 ade6⁻*	This work
AP3533	h⁺ *cdr2-mEGFP:kanMX6 leu1⁺:Pcdr2-cdr2-myc$_{12}$ ura4-D18 ade6⁻*	This work
AP4232	h⁺ *ura4⁺:cdr2N-kcc4C–myc$_{12}$*	This work
AP3956	h⁻ *cdr2N-kcc4C–GFP:kanMX6 ura4⁺:cdr2N-kcc4C–myc$_{12}$ leu1-32*	This work
Fig. 5		
AP3087	h⁻ *cdr2-mEGFP:kanMX6 leu1-32*	This work
AP3227	h⁺ *cdr2-mEGFP:kanMX6 leu1⁺:Pmid1-pom1-chimera–mCherry*	This work
AP2876	h⁺ *cdr2-mEGFP:kanMX6 pom1Δ::natMX6*	This work
Fig. 6		
AP3087	h⁻ *cdr2-mEGFP:kanMX6 leu1-32*	This work
AP3227	h⁺ *cdr2-mEGFP:kanMX6 leu1⁺:Pmid1-pom1-chimera–mCherry*	This work
AP3344	h⁻ *cdr2^{KD}-mEGFP:kanMX6 leu1-32*	Laboratory stock
AP3736	h⁻ *cdr2N-kcc4C–GFP:kanMX6 leu1-32*	This work
AP4241	h⁻ *cdr2N-kcc4C–GFP:kanMX6 leu1⁺:Pmid1-pom1-chimera–mCherry*	This work
AP3952	h⁻ *cdr2N^{KD}-kcc4C-GFP:kanMX6 leu1-32*	This work
AP3788	h⁺ *mid1-mEGFP:kanMX6 cdr2-TagRFP:natMX6 leu1-32 ura4-D18*	This work
AP4218	h⁺ *mid1-mEGFP:kanMX6 cdr2-TagRFP:natMX6 leu1⁺:Pmid1-pom1-chimera–HA$_3$ ura4-D18*	This work
AP4052	h⁻ *mid1-mEGFP:kanMX6 cdr2^{KD}-TagRFP:natMX6 leu1-32 ura4-D18*	This work
Fig. 7		
AP3081	h⁻ *GFP–cdr2-Cter:kanMX6 leu1-32 ura4-D18 ade6-M210*	This work
AP3062	h⁻ *GFP–cdr2-Cter:kanMX6 pom1Δ::natMX6 leu1-32 ura4-D18 ade6⁻*	This work
AP3055	h⁺ *GFP–cdr2-Cter:kanMX6 leu1⁺:Pmid1-pom1-chimera–mCherry*	This work
AP3503	h⁻ *GFP–cdr2-Cter$^{\Delta bsc}$:kanMX6 leu1-32*	This work

Table S1. **List of strains used in this study** *(Continued)*

Strain number	Genotype	Source
AP4417	h⁻ *GFP–cdr2-Cter$^{bsc\text{-}3D}$:kanMX6 leu1-32*	This work
AP4749	h⁻ *GFP–cdr2-Cter$^{bsc\text{-}3A}$:kanMX6 leu1-32*	This work
Fig. 8		
AP3087	h⁻ *cdr2-mEGFP:kanMX6 leu1-32*	This work
AP4462	h⁻ *cdr2$^{bsc\text{-}3D}$-mEGFP:kanMX6 leu1-32*	This work
AP4740	h⁻ *cdr2$^{bsc\text{-}3A}$-mEGFP:kanMX6 leu1-32*	This work
AP3724	h⁻ *cdr2-mEGFP:kanMX6 mid1Δ::ura4⁺ leu1⁺:Pmid1-mid1$^{Δ400–450}$*	This work
AP4442	h⁻ *cdr2$^{bsc\text{-}3D}$-mEGFP:kanMX6 mid1Δ::ura4⁺ leu1⁺:Pmid1-mid1$^{Δ400–450}$*	This work
AP4754	h⁻ *cdr2$^{bsc\text{-}3A}$-mEGFP:kanMX6 mid1Δ::ura4⁺ leu1⁺:Pmid1-mid1$^{Δ400–450}$ ade6⁻*	This work
AP3344	h⁻ *cdr2^{KD}-mEGFP:kanMX6 leu1-32*	Laboratory stock
AP4500	h⁻ *cdr2$^{KD\ bsc\text{-}3D}$-mEGFP:kanMX6 leu1-32*	This work
AP4746	h⁻ *cdr2$^{KD\ bsc\text{-}3A}$-mEGFP:kanMX6 leu1-32*	This work
AP4537	h⁻ *cdr2-mEGFP:kanMX6 mid1Δ::ura4⁺ leu1⁺:Pmid1-mid1^{nsm} ade6⁻*	This work
AP4756	h⁻ *cdr2$^{bsc\text{-}3A}$-mEGFP:kanMX6 mid1Δ::ura4⁺ leu1⁺:Pmid1-mid1^{nsm}*	This work
AP2876	h⁺ *cdr2-mEGFP:kanMX6 pom1Δ::natMX6*	This work
Fig. S1		
AP3087	h⁻ *cdr2-mEGFP:kanMX6 leu1-32*	This work
AP3112	h⁻ *cdr2^{bsc*}-mEGFP:kanMX6 leu1-32*	This work
AP3526	h⁻ *cdr2^{Δbsc}-mEGFP:kanMX6 leu1-32*	This work
AP3136	h⁻ *cdr2Δ::natMX6 leu1⁺:Pcdr2-cdr2^{hlx1*}-GFP*	This work
AP3140	h⁻ *cdr2Δ::natMX6 leu1⁺:Pcdr2-cdr2^{hlx2*}-GFP*	This work
AP3142	h⁻ *cdr2Δ::natMX6 leu1⁺:Pcdr2-cdr2^{hlx3*}-GFP*	This work
Fig. S2		
AP3087	h⁻ *cdr2-mEGFP:kanMX6 leu1-32*	This work
AP3428	h⁻ *cdr2^{FF*}-mEGFP:kanMX6 leu1-32 ura4-D18 ade6⁻*	This work
AP3112	h⁻ *cdr2^{bsc*}-mEGFP:kanMX6 leu1-32*	This work
AP3774	h⁻ *cdr2^{bsc*FF*}-mEGFP:kanMX6 leu1-32*	This work
AP3081	h⁻ *GFP–cdr2-Cter:kanMX6 leu1-32 ura4-D18 ade6-M210*	This work
AP4230	h⁻ GFP–*cdr2-Cter:kanMX6 mid1Δ::ura4⁺ leu1⁺:Pmid1-mid1$^{Δ400–450}$*	This work
Fig. S3		
AP2876	h⁺ *cdr2-mEGFP:kanMX6 pom1Δ::natMX6*	This work
AP3087	h⁻ *cdr2-mEGFP:kanMX6 leu1-32*	This work
AP4766	h⁺ *mid1-mEGFP:kanMX6 cdr2-TagRFP:natMX6 leu1-32 ura4-D18 pom1Δ::ura4⁺*	This work
AP3788	h⁺ *mid1-mEGFP:kanMX6 cdr2-TagRFP:natMX6 leu1-32 ura4-D18*	This work
AP3227	h⁺ *cdr2-mEGFP:kanMX6 leu1⁺:Pmid1-pom1-chimera–mCherry*	This work
AP3344	h⁻ *cdr2^{KD}-mEGFP:kanMX6 leu1-32*	Laboratory stock
AP3428	h⁻ *cdr2^{FF*}-mEGFP:kanMX6 leu1-32 ura4-D18 ade6⁻*	This work
AP3369	h⁺ *cdr2^{FF*}-mEGFP:kanMX6 leu1⁺:Pmid1-pom1-chimera–mCherry ura4-D18 ade6⁻*	This work
AP3768	h⁻ *cdr2$^{KD\text{-}FF*}$-mEGFP:kanMX6 leu1-32*	This work
AP3724	h⁻ *cdr2-mEGFP:kanMX6 mid1Δ::ura4⁺ leu1⁺:Pmid1-mid1$^{Δ400–450}$*	This work
AP4004	h⁻ *cdr2^{KD}-mEGFP:kanMX6 mid1Δ::ura4⁺ leu1⁺:Pmid1-mid1$^{Δ400–450}$ ura4-D18 ade6⁻*	This work
Fig. S5		
AP3087	h⁻ *cdr2-mEGFP:kanMX6 leu1-32*	This work
AP4462	h⁻ *cdr2$^{bsc\text{-}3D}$-mEGFP:kanMX6 leu1-32*	This work
AP4746	h⁻ *cdr2$^{KD\ bsc\text{-}3A}$-mEGFP:kanMX6 leu1-32*	This work
AP4462	h⁻ *cdr2$^{bsc\text{-}3R}$-mEGFP:kanMX6 leu1-32*	This work

Table S2. **List of plasmids used in this study**

Systematic name	Developed name	Details of expressed construct
Fig. 1		
pSR34	pFA6a-kanMX6-*Pcdr2-cdr2-mEGFP*	*cdr2-mEGFP*
pSR105	pFA6a-kanMX6-*Pcdr2-cdr2^{RKRKR*}-mEGFP*	*cdr2$^{R682Q\ K684N\ R685Q\ K692N\ R695Q}$-mEGFP*
pSR38	pFA6a-kanMX6-*Pcdr2-cdr2^{bsc*}-mEGFP*	*cdr2$^{K598N\ H599Q\ R600Q\ R601Q\ R602Q\ K612N\ K613N\ K614N}$-mEGFP*
pSR85	pFA6a-kanMX6-*Pcdr2-cdr2^{RR*}-mEGFP*	*cdr2$^{R624Q\ R628Q}$-mEGFP*
pSR122	pFA6a-kanMX6-*Pcdr2-cdr2$^{RR*-RKRKR*}$-mEGFP*	*cdr2$^{R624Q\ R628Q\ R682Q\ K684N\ R685Q\ K692N\ R695Q}$-mEGFP*
pSR121	pFA6a-kanMX6-*Pcdr2-cdr2$^{bsc*-RKRKR*}$-mEGFP*	*cdr2$^{K598N\ H599Q\ R600Q\ R601Q\ R602Q\ K612N\ K613N\ K614N\ R682Q\ K684N\ R685Q\ K692N\ R695Q}$-mEGFP*
pSR106	pFA6a-kanMX6-*Pcdr2-cdr2$^{\Delta bsc}$-mEGFP*	*cdr2$^{\Delta 591–619}$-mEGFP*
Fig. 2		
pSR25	pFA6a-kanMX6-*Pcdr2-GFP–cdr2-Cter*	*GFP-cdr2(591–747)*
pSR273	pFA6a-kanMX6-*Pcdr2-GFP–kcc4-Cter*	*GFP-kcc4(893–1,037)*
pSR160	pJK148-*Pcdr2-cdr2-Cter–myc$_{12}$, leu1$^+$*	*cdr2(591–747)-myc$_{12}$*
pSR152	pREP1-*GST–cdr2-Cter*	*GST-cdr2(591–747)*
pSR288	pJK148-*Pcdr2-kcc4-Cter–myc$_{12}$, leu1$^+$*	*kcc4(893–1,037)-myc$_{12}$*
pSR289	pREP1-*GST–kcc4-Cter*	*GST-kcc4(893–1,037)*
Fig. 3		
pSR25	pFA6a-kanMX6-*Pcdr2-GFP–cdr2-Cter*	*GFP-cdr2(591–747)*
pSR111	pFA6a-kanMX6-*Pcdr2-GFP–cdr2-Cter^{FF*}*	*GFP-cdr2(591–747)$^{F704D\ F705D}$*
pSR102	pFA6a-kanMX6-*Pcdr2-GFP–cdr2-Cter$^{\Delta bsc}$*	*GFP-cdr2(620–747)*
pSR160	pJK148-*Pcdr2-cdr2-Cter–myc$_{12}$, leu1$^+$*	*cdr2(591–747)-myc$_{12}$*
pSR161	pJK148-*Pcdr2-cdr2-Cter^{FF*}–myc$_{12}$, leu1$^+$*	*cdr2(591–747)$^{F704D\ F705D}$-myc$_{12}$*
pSR276	pJK148-*Pcdr2-cdr2-Cter$^{\Delta bsc}$–myc$_{12}$, leu1$^+$*	*cdr2(620–747)-myc$_{12}$*
pSR152	pREP1-*GST–cdr2-Cter*	*GST-cdr2(591–747)*
pSR153	pREP1-*GST–cdr2-Cter^{FF*}*	*GST-cdr2(591–747)$^{F704D\ F705D}$*
pSR277	pREP1-*GST–cdr2-Cter$^{\Delta bsc}$*	*GST-cdr2(591–619)*
pSR34	pFA6a-kanMX6-*Pcdr2-cdr2-mEGFP*	*cdr2-mEGFP*
pSR84	pFA6a-kanMX6-*Pcdr2-cdr2^{FF*}-mEGFP*	*cdr2$^{F704D\ F705D}$-mEGFP*
Fig. 4		
pSR34	pFA6a-kanMX6-*Pcdr2-cdr2-mEGFP*	*cdr2-mEGFP*
pSR135	pFA6a-kanMX6-*Pcdr2-cdr2N-kcc4C–GFP*	*cdr2(1–590)-kcc4(917–1,037)–GFP*
pSR84	pFA6a-kanMX6-*Pcdr2-cdr2^{FF*}-mEGFP*	*cdr2$^{F704D\ F705D}$-mEGFP*
pSR98	pJK148-*Pcdr2-cdr2-myc$_{12}$, leu1$^+$*	*cdr2-myc$_{12}$*
pSR163	pJK210-*Pcdr2-cdr2N-kcc4C–myc$_{12}$, ura4$^+$*	*cdr2(1–590)-kcc4(917–1,037)–myc$_{12}$*
pMA32	pJK148-*Pmid-mid1$^{\Delta 400–450}$, leu1$^+$*	*mid1$^{\Delta 400–450}$*
Fig. 5		
pSR34	pFA6a-kanMX6-*Pcdr2-cdr2-mEGFP*	*cdr2-mEGFP*
pAM18	pJK148-*Pmid1-pom1-chimera–mCherry, leu1$^+$*	*pom1(591–1,087)-mid1(500–920)–mCherry*
Fig. 6		
pSR34	pFA6a-kanMX6-*Pcdr2-cdr2-mEGFP*	*cdr2-mEGFP*
pAM18	pJK148-*Pmid1-pom1-chimera–mCherry, leu1$^+$*	*pom1(591–1,087)-mid1(500–920)–mCherry*
pMG52	pFA6a-kanMX6-*Pcdr2-cdr2^{KD}-mEGFP*	*cdr2^{E177A}-mEGFP*
pSR135	pFA6a-kanMX6-*Pcdr2-cdr2N-kcc4C–GFP*	*cdr2(1–590)-kcc4(917–1,037)–GFP*
pSR166	pFA6a-kanMX6-*Pcdr2-cdr2N^{KD}-kcc4C–GFP*	*cdr2 (1–590) ^{E177A}-kcc4(917–1,037)–mEGFP*
pSR182	pJK148-*Pmid1-pom1-chimera–HA$_3$, leu1$^+$*	*pom1(591–1,087)-mid1(500–920)–HA$_3$*
–	pFA6a-*TagRFP::NatMX6*	*TagRFP*
Fig. 7		
pSR25	pFA6a-kanMX6-*Pcdr2-GFP–cdr2-Cter*	*GFP-cdr2(591–747)*
pSR102	pFA6a-kanMX6-*Pcdr2-GFP–cdr2-Cter$^{\Delta bsc}$*	*GFP-cdr2(620–747)*
pAM18	pJK148-*Pmid1-pom1-chimera–mCherry, leu1$^+$*	*pom1(591–1,087)-mid1(500–920)–mCherry*
pSM1275	pMAL-TEV-*cdr2(518–620)*	MBP-TEV-*cdr2(518–620)*
pSM1294	pMAL-TEV-*cdr2(518–620)$^{bsc\text{-}4A}$*	MBP-TEV-*cdr2(518–620)$^{S604A\ S607A\ S616A\ S618A}$*
pSR219	pFA6a-kanMX6-*Pcdr2-GFP–cdr2-Cter$^{bsc\text{-}3D}$*	*GFP-cdr2(591–747)$^{S604D\ S607D\ S616D}$*
pSR282	pFA6a-kanMX6-*Pcdr2-GFP–cdr2-Cter$^{bsc\text{-}3A}$*	*GFP-cdr2(591–747)$^{S604A\ S607A\ S616A}$*
Fig. 8		
pSR34	pFA6a-kanMX6-*Pcdr2-cdr2-mEGFP*	*cdr2-mEGFP*
pSR231	pFA6a-kanMX6-*Pcdr2-cdr2$^{bsc\text{-}3D}$-mEGFP*	*cdr2$^{S604D\ S607D\ S616D}$-mEGFP*
pSR278	pFA6a-kanMX6-*Pcdr2-cdr2$^{bsc\text{-}3A}$-mEGFP*	*cdr2$^{S604A\ S607A\ S616A}$-mEGFP*
pSR255	pFA6a-kanMX6-*Pcdr2-cdr2$^{KD\text{-}bsc\text{-}3D}$-mEGFP*	*cdr2$^{E177A\ S604D\ S607D\ S616D}$-mEGFP*

Table S2. **List of plasmids used in this study** *(Continued)*

Systematic name	Developed name	Details of expressed construct
pSR280	pFA6a-kanMX6-*Pcdr2-cdr2$^{KD\text{-}bsc\text{-}3A}$-mEGFP*	*cdr2$^{E177A\ S604A\ S607A\ S616A}$-mEGFP*
pMA32	pJK148-*Pmid-mid1$^{\Delta 400–450}$, leu1^{+}*	*mid1$^{\Delta 400–450}$*
pMA49	pJK148-*Pmid-mid1^{nsm}, leu1^{+}*	*mid1^{nsm}*
Fig. S1		
pSR34	pFA6a-kanMX6-*Pcdr2-cdr2-mEGFP*	*cdr2-mEGFP*
pSR38	pFA6a-kanMX6-*Pcdr2-cdr2^{bsc*}-mEGFP*	*cdr2$^{K598N\ H599Q\ R600Q\ R601Q\ R602Q\ K612N\ K613N\ K614N}$-mEGFP*
pSR106	pFA6a-kanMX6-*Pcdr2-cdr2$^{\Delta bsc}$-mEGFP*	*cdr2$^{\Delta 591–619}$-mEGFP*
–	pJK148-*Pcdr2-cdr2^{hlx1*}-GFP, leu1^{+}*	*cdr2$^{F626A\ L627A\ F630A\ F631A}$-GFP*
pSR11	pJK148-*Pcdr2-cdr2^{hlx2*}-GFP, leu1^{+}*	*cdr2$^{L648A\ I652A\ V655A\ L656A\ W659A}$-GFP*
pSR12	pJK148-*Pcdr2-cdr2^{hlx3*}-GFP, leu1^{+}*	*cdr2$^{F720A\ L723A}$-GFP*
pSR165	pGEX6p1-*GST–cdr2-Cter*	*GST-cdr2(591–775)*
–	pGEX6p1	*GST*
Fig. S2		
pSR34	pFA6a-kanMX6-*Pcdr2-cdr2-mEGFP*	*cdr2-mEGFP*
pSR38	pFA6a-kanMX6-*Pcdr2-cdr2^{bsc*}-mEGFP*	*cdr2$^{K598N\ H599Q\ R600Q\ R601Q\ R602Q\ K612N\ K613N\ K614N}$-mEGFP*
pSR84	pFA6a-kanMX6-*Pcdr2-cdr2^{FF*}-mEGFP*	*cdr2$^{F704D\ F705D}$-mEGFP*
pSR120	pFA6a-kanMX6-*Pcdr2-cdr2^{bsc*FF*}-mEGFP*	*cdr2$^{K598N\ H599Q\ R600Q\ R601Q\ R602Q\ K612N\ K613N\ K614N\ F704D\ F705D}$-mEGFP*
pMA32	pJK148-*Pmid-mid1$^{\Delta 400–450}$, leu1^{+}*	*mid1$^{\Delta 400–450}$*
pSR25	pFA6a-kanMX6-*Pcdr2-GFP–cdr2-Cter*	*GFP-cdr2(591–747)*
Fig. S3		
pSR34	pFA6a-kanMX6-*Pcdr2-cdr2-mEGFP*	*cdr2-mEGFP*
pAM18	pJK148-*Pmid1-pom1-chimera–mCherry, leu1^{+}*	*pom1(591–1,087)-mid1(500–920)–mCherry*
pMG52	pFA6a-kanMX6-*Pcdr2-cdr2^{KD}-mEGFP*	*cdr2^{E177A}-mEGFP*
pSR84	pFA6a-kanMX6-*Pcdr2-cdr2^{FF*}-mEGFP*	*cdr2$^{F704D\ F705D}$-mEGFP*
pSR139	pFA6a-kanMX6-*Pcdr2-cdr2$^{KD\text{-}FF*}$-mEGFP*	*cdr2$^{E177A\ F704D\ F705D}$-mEGFP*
pMA32	pJK148-*Pmid-mid1$^{\Delta 400–450}$, leu1^{+}*	*mid1$^{\Delta 400–450}$*
–	pFA6a-*TagRFP::NatMX6*	*TagRFP*
Fig. S4		
pSM1192	pGEX-4T-1–*cdr2(518–620)*	*GST-cdr2(518–620)*
pSM1193	pGEX-4T-1–*cdr2(518–620)$^{604\text{-}607\text{-}2A}$*	*GST-cdr2(518–620)$^{S604A\ S607A}$*
pSM1194	pGEX-4T-1–*cdr2(518–620)$^{604\text{-}607\text{-}616\text{-}618\text{-}4A}$*	*GST-cdr2(518–620)$^{S604A\ S607A\ S616A\ S618A}$*
pSM1195	pGEX-4T-1–*cdr2(518–620)$^{616\text{-}618\text{-}2A}$*	*GST-cdr2(518–620)$^{S616A\ S618A}$*
pSM1196	pGEX-4T-1–*cdr2(518–620)^{618A}*	*GST-cdr2(518–620)^{S618A}*
pSM1318	pGEX-4T-1–*cdr2(518–620)$^{604\text{-}607\text{-}616\text{-}3A}$*	*GST-cdr2(518–620)$^{S604A\ S607A\ S616A}$*
pSM1319	pGEX-4T-1–*cdr2(518–620)$^{604\text{-}607\text{-}618\text{-}3A}$*	*GST-cdr2(518–620)$^{S604A\ S607A\ S618A}$*
pSM1310	pGEX-4T-1–*pom1*	*GST-pom1*
pSM972	pGEX-4T-1–*pom1^{KD}*	*GST–pom1-2*
Fig. S5		
pSR34	pFA6a-kanMX6-*Pcdr2-cdr2-mEGFP*	*cdr2-mEGFP*
pSR231	pFA6a-kanMX6-*Pcdr2-cdr2$^{bsc\text{-}3D}$-mEGFP*	*cdr2$^{S604D\ S607D\ S616D}$-mEGFP*
pSR278	pFA6a-kanMX6-*Pcdr2-cdr2$^{bsc\text{-}3A}$-mEGFP*	*cdr2$^{S604A\ S607A\ S616A}$-mEGFP*
pSR234	pFA6a-kanMX6-*Pcdr2-cdr2$^{bsc\text{-}3R}$-mEGFP*	*cdr2$^{S604R\ S607R\ S616R}$-mEGFP*

Table S3. **Cell length at division in mutants of the C-terminal–anchoring domain**

Strain	Genotype	Length at division
		μm
AP752	Wild type	13.5 ± 1.2 (148)
AP2804	*cdr2Δ*	17.9 ± 1.2 (315)
AP3087	*cdr2-mEGFP*	13.6 ± 0.8 (427)
AP3418	$cdr2^{RR*}$*-mEGFP*	13.4 ± 0.9 (349)
AP3568	$cdr2^{RKRKR*}$*-mEGFP*	15.4 ± 1.1 (324)
AP3526	$cdr2^{\Delta bsc}$*-mEGFP*	14.8 ± 1.1 (502)
AP3112	$cdr2^{bsc*}$*-mEGFP*	14.9 ± 0.8 (236)
AP3548	$cdr2^{RR*\text{-}RKRKR*}$*-mEGFP*	17.2 ± 1.1 (188)
AP3546	$cdr2^{bsc*\text{-}RKRKR*}$*-mEGFP*	17.7 ± 1.1 (214)
AP4249	$cdr2^{FF*}$*-mEGFP*	16.2 ± 1.1 (189)
AP3136	$cdr2^{hlx1*}$*-GFP*	18.4 ± 1.2 (108)
AP3140	$cdr2^{hlx2*}$*-GFP*	19.1 ± 1.3 (206)
AP3142	$cdr2^{hlx3*}$*-GFP*	18.7 ± 1.3 (163)

Mean length at division ± SD with (*n*) number of cells analyzed, grouped from three or more experiments.

Reference

Moravcevic, K., J.M. Mendrola, K.R. Schmitz, Y.H. Wang, D. Slochower, P.A. Janmey, and M.A. Lemmon. 2010. Kinase associated-1 domains drive MARK/PAR1 kinases to membrane targets by binding acidic phospholipids. *Cell*. 143:966–977. http://dx.doi.org/10.1016/j.cell.2010.11.028